ABSTRACT

Title of dissertation: RELAXATION AND STIFFENING DYNAMICS OF A SINGLE SEMIFLEXIBLE POLYMER CHAIN

Inuka D. Dissanayake,
Doctor of Philosophy, 2006

Dissertation directed by: Professor Panagiotis Dimitrakopoulos
Department of Chemical and
Biomolecular Engineering

Both synthetic and biological polymers are a challenge to study because of the many features and functional roles they carry. A good understanding of the macromolecule's dynamical properties is essential for biological processes such as the cytoskeleton dynamics of actin or in creating novel materials such as biodegradable nanocomposites. Here we focus on the Brownian dynamics of single semiflexible polymer chains, specifically the relaxation and stiffening behaviors. To date, the transient modeling of dilute solutions has concentrated mainly on flexible chains. Semiflexible polymers, with a persistence length comparable to or larger than their contour length show distinct properties in solution.

Brownian dynamics simulations based on a discretized version of the Kratky-Porod chain model were employed. First, the relaxation of a bead-rod polymer chain from an initially straight configuration was followed. Through a scaling-

law analysis, universal relaxation laws were determined covering all time scales. A correlation describing the properties studied by the single parameter of chain length was noticed. Based on this, we were able to confirm and explain the chain's stress and optical properties, as well as derive a nonlinear stress-optic law valid for semiflexible chains at any time period. Also, we determine the relaxation for long semiflexible chains exhibit two intermediate-time behaviors, as a result of the interplay of Brownian and bending forces on the link tensions.

A second project involved the relaxation dynamics of a worm-like bead-spring chain. Existing relaxation simulations of this bead-spring model are limited to the stress behavior. Here we monitor the short and intermediate-time relaxation behaviors of a nearly extended semiflexible chain. We also look at the effects of the Kuhn length on a chain of constant length.

Finally, the interesting behavior of the coil-helix-rod stiffening transition was studied. When subjected to external forces or a change in solution conditions the macromolecule may stiffen. Being able to control the chain stiffness is of technological importance especially for nanotechnology devices where the constraint of the walls limits the entropy available to the chain. We have successfully simulated the transient conformational behavior and subsequently understand the chain dynamics involved through analysis of the chain's length, width, and stress.

RELAXATION AND STIFFENING DYNAMICS OF A SINGLE SEMIFLEXIBLE POLYMER CHAIN

by

Inuka D. Dissanayake

Dissertation submitted to the Faculty of the Graduate School of the
University of Maryland, College Park in partial fulfillment
of the requirements for the degree of
Doctor of Philosophy
2006

Advisory Committee:

Professor Panagiotis Dimitrakopoulos, Chair
Professor Sheryl H. Ehrman
Professor Peter Kofinas
Professor Luz Martinez-Miranda
Professor Srinivasa R. Raghavan

ACKNOWLEDGEMENTS

First and foremost I would like to thank my advisor, Professor Panagiotis Dimitrakopoulos, for his support, encouragement, and most of all patience as I went through this journey of growing and learning. I would also like to acknowledge my committee members, Professors Sheryl Ehrman, Peter Kofinas, Luz Martinez-Miranda, and Srinivasa Raghavan for their valuable time and insight.

I am grateful for Dr. Dimitrakopoulos' group members, my close friends, and my family, all of whom have played an important role in helping me to get to this point. Special thanks to Jon and Q, both of you knew when I needed to be pushed and reminded of my dreams. Finally, I thank God, for without His love I would not be who I am.

Table of Contents

List of Tables

List of Figures

Chapter 1

Polymer Physics

1.1 Introduction

Polymers are one of the most commonly used class of material in today's world. The diversity of this material is seen by its application in the food, plastic, defense, pharmaceutical and various other industries. Polymers can be divided into two groups, synthetic polymers and biopolymers. Synthetic polymers are known as man-made polymers because of the scientist's ability to control the synthesis and growth of the macromolecule. Teflon, nylon, polycarbonate, and polyethylene are some of the common names that describe such polymers. In contrast, biopolymers occur naturally and are found in living organisms. Examples of biopolymers include the tobacco mosaic virus, cellulose, DNA, actin filaments, and microtubules. A good understanding of the polymer's dynamical properties is essential towards

the study of biological processes such as the cytoskeletal dynamics of actin [12] or the dynamics of protein deposition on implant materials [48], or in creating novel materials such as enhanced flat panel displays [53] or biodegradable nanocomposites [58].

Because of the many features and functional roles they carry, both synthetic and biological polymers are a challenge to study. This challenge is proven true by noticing the many different experimental techniques such as fluorescence microscopy, electrophoresis, light scattering, optical microscopy, force spectroscopy, and viscometry [49, 54, 55, 65, 68], along with the different simulation methods ranging from Monte Carlo to Brownian dynamics, bead-spring models to bead-rod models, and shear to extensional flow studies [19, 40, 59], used to gain insight on the different properties of the macromolecule.

Here we are concerned with the physics of single semiflexible polymer chains. In particular, the transient bead-rod and bead-spring chain properties are examined to understand the dynamics of the chain under various dilute solution conditions. A dilute solution is defined such that the chain is surrounded by solvent molecules and there is no chance of contact with another chain. The non-Newtonian properties of the chain are captured through a Brownian dynamics study. Among the properties studied are the chain length, stress, tension, and the birefringence; all these properties can help give the full picture of chain conformation and behavior in solution.

In the past, attention has been mainly focused on flexible polymers. Semiflexible polymers however, with a persistence length comparable to or larger than their contour length, show distinct properties in solution. Examples of biopolymers, in order of increasing stiffness, are DNA, actin, microtubules, and collagen. Some properties of these biomolecules include: DNA, molecular weight (MW) of 10^8 with a polymer persistence length of only 50 nm; actin, MW of 42,000 with a persistence length of about 1.5-20 μm; the monomer MW of microtubules is 110,000 and the persistence length is up to 7 mm; finally, the stiff biopolymer collagen is known to have a monomer weight of 300,000 with a persistence length of 14.5 nm. Common examples of semiflexible synthetic polymers include Kevlar, polyvinyl chloride (PVC), polyamide (nylon), and polyesters. The stiffness shown in these polymers results in unique properties of their solutions. For example, the importance of the semiflexibility in F-actin can be seen by recognizing that as the persistence length increases the polymer bundles and adsorbs onto surfaces easily [37]. In the case of synthetic polymers, the aromatic and amide molecular groups in Kevlar result in its common use of providing strength for light-weight materials.

Three simulation projects have been studied in this thesis. First, the relaxation of bead-rod polymer chains with both chain stiffness and the chain length being the adjustable parameters. Polymer behavior of an initially extended chain was monitored and through scaling-law analysis universal relaxation laws were

determined for semiflexible chains. Studies of the stiff relaxation behavior show the long chains exhibit two intermediate behaviors due to the presence of bending energy. A correlation was noticed such that the properties studied can be predicted by the single variable of chain length. Because of this correlation, we were able to also define a non-linear stress-optic law valid for stiff chains at all time periods.

The second project, describes detailed simulation results for the relaxation of the worm-like bead-spring chain. Existing simulations of the relaxation of this bead-spring model are limited. The short and intermediate-time relaxation behavior of this polymer model has been predicted.

Finally, the behavior of chain stiffening is also studied. When subjected to external forces such as strain or a change in solution conditions such as an ionic strength decrease the polymer chain, synthetic polymer or biopolymer, may stiffen experiencing a helical conformation before reaching the final rod like state. By being able to control the chain rigidity, researchers may create better trapping gel networks, micro-electronic devices from plastics or novel drug delivery systems [52]. The increase in the chain persistence length L_p or chain Kuhn length affects the polymer conformation and consequently its behavior in solution. We have successfully simulated the behavior and are able to see the coil-helix-rod transition and subsequently understand the chain dynamics through analysis of the chain's three eigenvalues and the first normal stress component.

1.2 Overview of Chapters

This thesis is organized as follows. Chapter 2 presents a review on various polymer simulation techniques, the development of the two polymer chain models we are interested in, along with their governing equations, and details of our Brownian dynamics simulation method. Definitions of the properties of interest and a comparison to experimental results are also discussed. Next, in Chapter 3, we first present a background literature review on bead-rod relaxation studies followed by our simulation results. Here we discuss and explain the results of using the bead-rod model to predict polymer relaxation behavior for short and long stiff chains. Similarly, Chapter 4 treats the relaxation study when the chain is modeled as a worm-like chain. Using this bead-spring model, we determine the relaxation dynamics at short and intermediate-times for semiflexible chains. In Chapter 5, the results of adding a bending energy to an initially coiled bead-rod chain is reported. An understanding of the dynamics of the coil-helix-rod behavior is presented through analysis of the chain's three eigenvalues and the first normal stress component. The main conclusions of each study are reiterated in Chapter 6. Finally, Chapter 7 discusses possible future work for the study of polymer physics through the use of Brownian dynamics.

Chapter 2

Numerical Method

Computational modeling can be applied to an array of polymer systems ranging from dilute or concentrated solutions to polymers in confined geometries. A recent increase in interest of simulations can be attributed to advances in computational power and computational resources. When the simulation method is not too intensive one can test extreme cases such as longer or stiffer chains, as well as monitor a wide range of molecular properties that otherwise might be limited in experimental studies. The main setback is computing time, which can be minimized with the use of supercomputers.

In this Chapter, we will give an overview on Brownian dynamics, describe both the bead-rod and bead-spring models, explain our simulation method, and show that both models agree well with past experimental and numerical observations.

2.1 Introduction

Many possible numerical methods exist for the study of polymer solutions, predominantly molecular dynamics and Brownian dynamics. Molecular dynamics is a great tool for understanding a polymer system at the atomic scale [26, 38] while Brownian dynamics is more commonly used when a continuous system is of interest.

In molecular dynamics, both the chain and solvent molecules of the model are represented on an atomic level. Calculating the particle-particle interactions, as well as accounting for any interaction potentials is time consuming, hence this method is primarily used to study the short-time properties of the polymer system. Newton's equation of motion is used to solve the model. While molecular dynamics has been around for decades, limitations exist in being able to study the behavior of chains of long length.

On the other hand, a continuum model allows one to disregard the difficulties in simulating explicit solvent forces and instead consider the solvent as a continuous incompressible fluid that exerts stochastic interactions on the polymer. The random or irregular collisions of the polymer with the many small solvent molecules is what defines the Brownian motion. One such stochastic numerical method is Brownian dynamics simulation. Not only do the beads experience drag, they also are under constant thermal bombardment by the solvent molecules. To get a good idea of the polymer's behavior under the effect of this force an average must be

taken over an ensemble of chains. The Langevin equation of motion accounts for the chain's intramolecular forces, as well as the stochastic force. Because of its continuous nature Brownian dynamics simulations require less computational time than molecular dynamics and allow for capturing the overall polymer behavior, hence it will be our simulation method of choice. We simulate the macromolecule under theta solvent conditions based on the Brownian dynamics method developed by Grassia & Hinch [33].

Brownian dynamics simulations have been used by many researchers in recent years to further understand the dynamics of polymer chains, an overview of the literature on this method will be covered in later chapters.

2.2 Model Description

Two non-linear models are considered for our Brownian dynamics studies, the bead-rod and the bead-spring models. The main difference between the two is the scale of resolution, where a spring in the bead-spring model represents many Kuhn lengths while a link in the the bead-rod model only represents a Kuhn length [44]. Brownian dynamics simulations based on a discretized version of the Kratky-Porod wormlike chain model, were employed. In both models the polymer is represented as massless $N + 1$ beads connected by N links or springs.

2.2.1 Bead-rod model

Until recently the use of the bead-rod model has been limited due to the necessary constraints on the link lengths. The Brownian dynamics method we present here is based on a modified version Grassia and Hinch [33] described for a flexible bead-rod model. By adding pseudo-potential forces, Grassia and Hinch converted the statistics of the system from that of a rigid link to an infinitely stiff bead-spring system allowing for equal probability of the chain angles and solving for the bead motion through the midstep method. With the bead-rod chain now at equilibrium there is no longer a need to equilibrate the initial conformation thereby minimizing computational time.

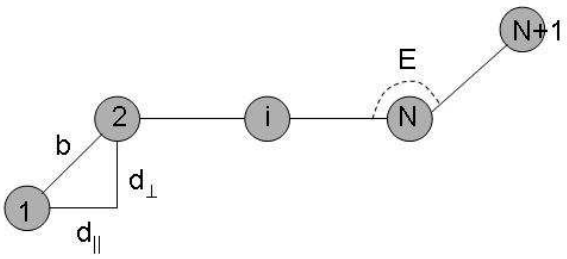

Figure 2.1: Bead-rod representation of a macromolecule.

As seen in figure 2.1, to represent the macromolecule, the chain is modeled as a sequence of beads connected by rigid rods. The freely-jointed chain is composed of $N + 1$ massless beads, each representing a few monomers, connected by N links of fixed bond length b allowing the contour length of the polymer to always be fixed. For a fixed link length, b, the properties of the polymer chain are defined by the number of links N and the bending energy E. The rods act as a constraint holding the beads at a set distance, while the beads themselves act to provide friction for the chain. The beads experience Brownian motion and consequently are under constant bombardment from the solvent molecules. The length of the links corresponds to the Kuhn length. Because the bond length is fixed, the transverse link length can be related to the longitudinal link length such that $d_\perp^2 = b^2 - d_\parallel^2$, and consequently the chain's length $R_\parallel$, since $R_\parallel \sim N d_\parallel$.

To study the behavior of stiff chains a bending energy term $\mathcal{E}$ is included. The bending energy is proportional to the square of the chain's local curvature

$$\phi^{bend} = \frac{1}{2}\,\mathcal{E}b \int_0^L \left(\frac{\partial^2 \boldsymbol{X}}{\partial s^2}\right)^2 \mathrm{d}s. \tag{1}$$

Since the chain stiffness is governed by the angle θ_i between two consecutive links, the bending energy of the discrete model can be defined as

$$\phi^{bend} = \mathcal{E}\sum_{i=1}^{N}(1-\cos\theta_i). \tag{2}$$

The bending energy is related to the chain persistence length L_p by $\mathcal{E}/k_BT = L_p/b$, where k_B is the Boltzmann constant. Based on this relation the dimensionless chain bending parameter becomes $E = \mathcal{E}/k_BT$. As the bending energy increases, the chain model goes from a freely-jointed to a rigid-rod model.

2.2.2 Bead-spring model

The bead-spring polymer model is a widely used polymer model. The Hookean dumbbell model is the simplest model and is described as two beads connected by a linear spring force. In this model the springs represent an elastic force in the polymer while the drag force is accounted for by the two beads. The simple

force law is described as $\mathbf{F}_i = Hd_i$ where the spring constant H is defined as $H = \frac{3k_BT}{b_k^2}$. A more realistic model is the finitely extensible nonlinear elastic (FENE) spring model, where the nonlinear spring potential serves to limit the maximum extension of the springs. Warner [71] described the force law as

$$\mathbf{F}_i = H\frac{d_i}{1-\left(\frac{dmag_i}{clen_i}\right)^2} \tag{3}$$

with a restriction of $dmag < clen$, i.e. the connecting vector can not exceed the maximum allowed spring extension. If the rate of stretching by a single spring is faster than the chain stretching then the bead-spring model is no longer an appropriate representation of the polymer.

Unlike the FENE or Hookean model the worm-like chain model (WLC) has not received as much computational attention. The worm-like chain has been proven to successfully describe the force-extension behavior of DNA molecules [8]. The mechanics of this model is based on the following spring law recognized by Marko and Siggia [47]

$$\mathbf{F}_i = \frac{Hd_i}{6dmag_i}[\frac{1}{\left(1-\frac{dmag_i}{clen_i}\right)^2} - 1 + \frac{4dmag_i}{clen_i}]. \tag{4}$$

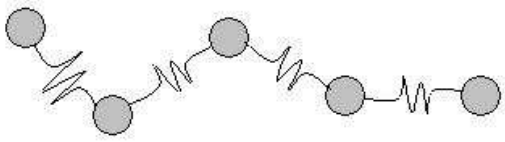

Figure 2.2: Bead-spring representation of a macromolecule.

We model the polymer such that the chain, again with $N + 1$ massless beads, is now connected by N springs, see figure 2.2. Unlike the bead-rod model the springs connecting the beads represent many Kuhn steps. To avoid unrealistic behavior, due to large fluctuations of the chain length, similar to the FENE model, care must be taken to ensure that the spring length does not exceed the maximum bond length.

2.3 Simulation Method

For both stiff chains and extended chains, hydrodynamics has little effect on intrachain dynamics, however, the force can be included if needed for studying other systems such as in the presence of flow fields [3, 34].

Summing the forces acting on each bead i and neglecting bead inertia leads to the first-order differential Langevin equation

$$\zeta \frac{\mathrm{d}\boldsymbol{X}_i}{\mathrm{d}t} = \boldsymbol{F}_i^{rand} + \boldsymbol{F}_i^{ten} + \boldsymbol{F}_i^{cor} + \boldsymbol{F}_i^{bend} \tag{5}$$

where $\boldsymbol{X}_i$ is the position vector for bead i and the length of each link is expressed as $\boldsymbol{d}_i = \boldsymbol{X}_{i+1} - \boldsymbol{X}_i$. The friction coefficient ζ is related to the solvent viscosity η_s by the relation $\zeta_i = 6\pi\eta_s b_i$ and because the bead radius b_i is set to be constant for all beads the friction coefficient is assumed to be uniform. $\boldsymbol{F}_i^{rand}$ is the Brownian force experienced by the beads due to the constant random bombardments of the solvent molecules. To get a good idea on the behavior of the polymer chain we take many statistically independent realizations. To produce random numbers for each realization, we re-initialize the random seed for each run generating numbers that are statistically independent and uniformly distributed. The random force is calculated only at the start of each time step such that $\langle \boldsymbol{F}_i^{rand} \boldsymbol{F}_i^{rand} \rangle = 2k_B T\zeta/\Delta t$. The tension force $\boldsymbol{F}_i^{ten}$ serves to maintain a fixed link length with the presence of constraining tensions T_i on each link such that $\boldsymbol{F}_i^{ten} = T_i \boldsymbol{d}_i - T_{i-1}\boldsymbol{d}_{i-1}$. For the

bead-spring model since there is no fixed link length the tension force is replaced by a spring force as described in Eq. (2). To make the equilibrium probability distribution of the bead-rod chain configurations Boltzmann a corrective potential force $\boldsymbol{F}_i^{cor} = -\nabla_i(k_B T \ln\sqrt{det})$ is added, where det is the determinant of a NxN tridiagonal symmetric matrix. Finally, the bending force $\boldsymbol{F}_i^{bend}$ is derived from the chain bending energy $\boldsymbol{F}_i^{bend} = -(\partial\phi^{bend}/\partial\boldsymbol{X}_i)$.

All physical properties mentioned from here on have been non-dimensionalized. Due to the ever present Brownian forces, a time scale related to the diffusive motion of a single bead, $\tau_{rand} = \zeta b^2/k_B T$ is used to represent a unit of time. Length values are scaled with b, forces by $k_B T/b$, and stresses by $k_B T$. As mentioned earlier, the relevant parameters of this study end up being the number of links and the bending parameter.

The Langevin equation is solved for new bead positions by the midpoint method in $O(N)$ operations [33]. Care must be taken in determining the time step. The size of the time step can affect the accuracy of the solution if it is too big. To make sure the time step is small enough, we make it 10^{-2} times smaller than the smallest time scale present in the problem, however, a very small time step has the disadvantage of requiring longer computational time. To account for the randomness brought on by Brownian motion, we take ensemble averages of up to 10,000 chains to get a clear picture of the polymer chain's dynamic properties. The shorter length chains are studied using larger ensemble averages with a still

small enough computing time (3-48hrs) on the Pentium IV cluster in our research group. Through the use of supercomputers at the National Center for Supercomputing Applications (NCSA) in Illinois, longer chains with a strong bending energy are able to be considered in a timely manner. To reduce computational time, the program is parallelized using Message Passing Interface (MPI) and executed on the distributed memory PC superclusters, namely Platinum, Tungsten, and Teragrid. With the use of up to 160 Intel Pentium III processors or 320 Intel Xeon processors results were obtained within a few days.

2.4 Properties

Despite the complexity at the molecular level, the macroscopic properties of polymer chains are influenced by characteristic length scales that are comparable to the persistence length of the molecules. Among the properties of interest in this dissertation are the chain eigenvalues, stresses, and birefringence; these properties help give the full picture of the chain conformation when placed under different solution conditions.

2.4.1 Configuration

By looking at a function that involves all the length scales of the macromolecule from that of the single bead to the entire chain, the chain evolution over extended time periods can be determined. Such a function is seen in the eigenvalues of the gyration tensor

$$\boldsymbol{R}_G^2 = \frac{1}{N_B}\sum_{i=1}^{N_B}(\boldsymbol{X}_i - \boldsymbol{X}_c)(\boldsymbol{X}_i - \boldsymbol{X}_c) \tag{6}$$

where $\boldsymbol{X}_c = \sum_{i=1}^{N_B} \boldsymbol{X}_i/N_B$ is the center of mass of the chain [14].

Of the three eigenvalues, the first, or largest, eigenvalue $R_{G,1}^2$ measures the chain length along its major axis and is used to monitor the polymer longitudinal length $R_\parallel$ (see figure 2.3). The other two eigenvalues, $R_{G,2}^2$ and $R_{G,3}^2$, measure the chain's size along its two minor axes and provide information about the chain width $R_\perp$. Note that $R_{G,1}^2 \sim R_\parallel^2$ and $R_{G,2}^2 \sim R_\perp^2$.

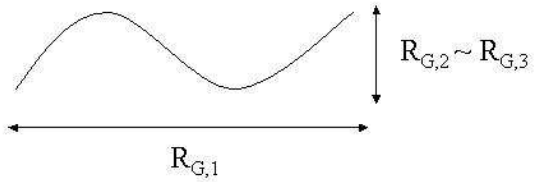

Figure 2.3: Polymer chain eigenvalues from the gyration tensor.

2.4.2 Stress

Looking at the stress contribution from the polymer chain can further help to understand the chain's configuration behavior. The stress tensor given as

$$\boldsymbol{\sigma} = -\sum_{i=1}^{N_B} \boldsymbol{X}_i \boldsymbol{F}_i^{total} \tag{7}$$

reveals how the forces are present across the chain. Here $\boldsymbol{F}_i^{total}$ is the sum of the forces acting on each bead as mentioned in Eq. (5). The tensor is affected by the polymer deformation, while at equilibrium it is isotropic.

2.4.3 Birefringence

Another property of interest is the birefringence of the solution. Birefringence is formally defined as the double refraction of light, which occurs with solution anisotropy. The term anisotropy refers to a non-uniform spatial distribution of properties, resulting in different values being obtained when a sample is probed from several directions. A ray of light incident on a birefringent material splits the beam into two rays. Anisotropic crystals, such as quartz or calcite, have distinct axes and interact with light by a mechanism that is dependent upon the orientation of the crystalline lattice with respect to the incident light angle. On the other hand, many transparent solids are optically isotropic, meaning that the index of refraction is equal in all directions throughout the crystalline lattice. Examples of isotropic solids include glass, table salt, diamond, and a wide variety of both organic and inorganic compounds. Light entering an isotropic material is refracted at a constant angle and passes through at a single velocity without being polarized.

Changes in the solution birefringence offer insight into chain orientation. The property is induced through stress from the movement of the local chain segments in solution, therefore, the straighter the chain the more birefringent the solution becomes. As a straight chain the maximum birefringence value for the bead-rod model is N. Computationally the indices of refraction of the rays are exploited to learn about the solution's birefringence. The relaxation of the chain's tensions

causes local changes to the index of refraction. The anisotropies of each segment is added to get the refractive index tensor

$$\boldsymbol{n} = \sum_{i=1}^{N} \hat{\boldsymbol{d}}_i \hat{\boldsymbol{d}}_i \tag{8}$$

where $\hat{\boldsymbol{d}}$ is the unit link length [50]. Knowing the refractive index components one can then calculate the birefringence by

$$B = \sqrt{(n_{11} - n_{22})^2 + 4(n_{12})^2} \tag{9}$$

where 1 and 2 are the two rays.

2.5 Comparison to Experiments

If we were to make a comparison of our bead-rod model to a λ-phage DNA molecule of contour length 21.2 μm and Kuhn length of approximately 0.132 μm [65] then we see that a chain consisting of 150 beads, or Kuhn steps, means b_k= L/N_k = 21.2/150 = 0.141 μm which proves to be a close description for the λ-phage DNA molecule. Hence in our studies, because the Kuhn length is kept constant, chains with fewer beads represent fragments of the biomolecule while chains with beads greater than 150 represent longer molecules.

A comparison of Brownian dynamics simulations with experimental measurements of polymer chains subjected to a flow field has been done by Larson *et al.* [44]. Here the authors successfully concluded the agreement of simulation and experimental measurements for DNA chains under extensional flow. Larson *et al.* not only numerically studied the unraveling dynamics of a single bead-spring flexible chain but also compared the results to the recent experimental findings of Perkins *et al.* [57] and Smith *et al.* [64]. The experimental studies, performed by Chu's group, consisted of analyzing the transient extension behavior of a fluorescently stained flexible lambda bacteriophage DNA (λ-DNA) molecule. Excellent agreement was noted and because of the extra information obtained computationally, the group was able to further conclude that the initial state of the chain does influence the unraveling path it takes. The stronger flow rate dominates over the Brownian motion, therefore the initial configuration is affected more by the drag

force, which can be seen by noticing the rapid full extension of the dumbbell chain under a stronger flow.

In contrast, with the use of Brownian dynamics simulations Jendrejack and co-workers [34] reproduced the experimental relaxation time of a stained DNA molecule. They defined the DNA molecule using the WLC model and included both hydrodynamic interactions (HI) and excluded volume (EV) effects. The experimental relaxation time of $4.1sec$ was reproduced by setting $b_k = 0.106\mu m$. A comparison to the extensional results of the Chu group [65] also, coincided well.

A similar observation of chain deformation was done by Li *et al.* [45]. Here they compared the results of previous experimental findings to their simulation results of dilute DNA and polystyrene solutions under shear flow. A comparison of the two methods showed that there is excellent agreement for DNA molecules while an over-prediction of polystyrene deformation was noticed. The authors suggested this difference in results for polystyrene molecules could either be due to the differences between the solvent effects on DNA and polystyrene molecules or an inaccuracy in the experimental method. They noted that while microscopy allows for direct observation of the polymer conformation, the indirectness of light scattering can only provide a bulk measure of microstructural information.

Another successful comparison on the transient study of DNA molecules was discussed by Dimitrakopoulos [15]. In that study, the simulated chain conformations and chain rotation were consistent with the experimental findings of Perkins

et al. [55]. Qualitative agreement was also noted in the long-time exponential decay exhibited by the relaxing chain. The comparison of Brownian dynamics results to theoretical predictions and experimental findings of stiff chains has also been done. With the use of the bead-rod model, Dimitrakopoulos *et al.* [13] accurately described the linear stress relaxation of flexible DNA molecules and semiflexible F-actin molecules.

Finally, Shankar *et al.* [62] simulated biopolymers and synthetic polymers of varying stiffness and also compared their results to existing experimental data. The authors noticed excellent agreement with earlier experimental work for the viscoelastic measurements of dilute solutions. The successful observation of single polymer chains in experiment and simulation allow for us to expand the study towards semiflexible chains.

Chapter 3

Relaxation of a Bead-Rod Chain

In this chapter, we consider the relaxation of initially straight semiflexible bead-rod chains. This study is motivated by the recent work of researchers using manipulation techniques with tethered beads and advanced imaging techniques through fluorescent staining to observe the time-dependent conformational dynamics of polymer chains such as DNA or polystyrene. Experimental studies followed the transient behavior of DNA collapsing after extension [55], or the motion of fluorescent stained actin filaments guided by molecular motors [39]. The direct visualization of molecules in solution was a breakthrough, no longer limiting the study of polymer rheological properties to their static behavior. Not only are the properties of the chain at equilibrium of interest, but how the chain coils back and the change in properties along the way to equilibrium is of significance.

Here the relaxation of a single semiflexible polymer chain from an initial straight configuration is studied. Physically this problem may correspond to a polymer chain being fully stretched by a strong flow, switching the flow off and then observing the chain relax towards equilibrium. The aim of this study is to fully understand the polymer conformation, stress, and optical transient behavior. The configuration relaxation has been determined over extended time periods through monitoring of the eigenvalues of the gyration tensor and application of the scaling law methodology. By studying the chain's lengths, the molecular conformation information gained was subsequently used to examine the stress and optical relaxation course of the semiflexible chain. Studying these chain properties as the chain relaxes from an initially extended state can provide insight, for example, as to how the polymer molecule functions within the cell influencing cell characteristics and behavior.

The path back to equilibrium is also of importance to many rheological problems encountered in industry. Under a strained force, such as an extensional flow, the macromolecule will deform. Once the strain is released, the chain will undergo a transition from that of a stretched state to a coiled phase affecting properties which depend on the polymer configuration. Recognizing the dynamics of the macromolecule as it relaxes is the first step towards understanding the behavior and manipulation of chains in confined spaces such as microfluidic devices. The results of this study can also improve our understanding towards the applica-

tion of polymeric materials in Micro-Electro-Mechanical Systems (MEMS), and pharmaceutical and biomedical processes.

3.1 Introduction

Progress on the study of polymer physics has been made from theory to experimental work to present day simulation work. Here we will review some of the significant experimental results on polymer relaxation and Brownian dynamics simulations on the bead-rod model.

Chu's group [55] set out to experimentally find scaling relations for the dynamic properties of single molecules by studying their dependence with time. By attaching one end of the chain to a bead, the chain was able to be manipulated with optical tweezers, and molecular motion of the stained DNA was directly observed through an optical microscope. The trapped bead was held stationary as single molecules of DNA were stretched to full extension by a flow velocity of 20 $\mu m/s$. Once flow was stopped fluorescent images were recorded, directly measuring the relaxation of the chain. Configuration changes showed an initially fast relaxation of the free end to 70% of its length, followed by a slower relaxation time as the chain reached its equilibrium coil-like state. Points of increased fluorescence intensity were noted along the chain, signaling the presence of knots, or overlap of molecules, during the relaxation process. Data was analyzed with inverse Laplace transformations to get a spectra of exponential decay and with data collapse to measure scaling relations. The longest relaxation time followed a scaling law of $\tau \approx L^{3\nu}$, with the scaling exponent measured to be 1.66. As expected the peaks of the relaxation spectrum did not match with the Rouse or Zimm theory [22]. Since

these two theory models describe behavior at equilibrium. The data were rescaled with time and length to arrive at a relation dependent only on the single variable of length. The linear behavior showed scaling agreement with results from the Laplace transform.

The experimental findings on the transient behavior of single DNA molecules led the way to further investigate properties of single molecules with an ultimate goal of understanding polymer dynamics. A stretched flexible polymer chain, in addition to experiment, can be simulated through Brownian dynamics to measure its relaxation properties. The simulation work of Hinch and coworkers [33] on the relaxation of polymer stresses lead the Brownian dynamics study of bead-rod models. Using the Langevin equation with a small enough time step to integrate the ODE, Brownian motion was simulated and stress was calculated according to Kramers' stress formula for chains of up to 100 beads in length. For a straight chain configuration the stress was measured and found to scale on the order of N^3. The authors saw the first normal component of stress decay by a power law at intermediate times, and finally an exponential decay at long times. The initial slow decay, can be explained by the large Brownian forces present causing sideways diffusion of the beads. At long times a more rapid exponential decay was noticed. Here the relaxation is dominated by the decay of the longitudinal extension of the chain. Their results show that even though the chain relaxes back to its equilibrium state, the long time relaxation scales differently from the Rouse

model. The relaxation rate was found to be higher than the predicted value. They base this difference on the existence of a quasi-static balance between link tensions and bead diffusion. Neglecting excluded volume had no effect on the results.

Further studies on the relaxation transient dynamics of bead-rod chains were performed by Doyle *et al.* [21]. The authors extended bead-rod chains in various linear flow fields and then monitored the relaxation behavior of the polymer. The observed stress relaxation data was in agreement with the results of Grassia and Hinch. The short time birefringence relaxation was also studied and a hysteresis was found between the stress and birefringence behavior of the bead-rod model.

Hatfield and Quake [31] focused on the effects of the forces involved in the relaxation process of single chains. They showed the tension force dominating over hydrodynamics through theory, simulation of a bead-rod chain of 21 beads, and comparison to the experimental results of the Chu's group. Because both tension forces and hydrodynamic interactions were included, the Rouse model was used to separate the effects of the two. By looking at the direct influence of extension on chain dynamics, the authors concluded that due to anisotropy, caused by extension, the polymer relaxation time splits into two components. A longitudinal and transverse time scale is observed. Due to symmetry at the coiled state only one relaxation time is observed at equilibrium. They were also able to see the influence of tensions over hydrodynamics on the relaxation time. As chain extension is varied the change in the tension forces influences the relaxation time

more noticeably than hydrodynamics.

Andrews *et al.* [4] heightened the bead-rod study by looking into the effects of a new variable. What made their research interesting was the inclusion of chain stiffness. Using the bending constant of the chain as the independent variable in the simulations the authors predicted the influence of chain flexibility on chain conformation. The authors not only studied the effect of steady and shear-flow but also looked into the relaxation properties of a seven-bead chain at short times. The relaxation studies revealed how an increase in stiffness leads to an increase in the chain's relaxation time. The effect of the tension and bending forces were more evident for the semiflexible chains by means of bumps on the data, while the rigid rods had a single curve, due to the dominance of its bending force over tension; proving the influence rigidity has on the chain's conformational and rheological properties.

3.2 Results and Discussion

While flexible relaxation dynamics has been studied both experimentally and computationally, the transient dynamics of semiflexible chains remains poorly understood over all time scales. As was seen by the review on Andrews *et al.* [4], flexibility of the chain does influence the rheological properties. Relaxation studies involving the bead-rod model are limited by not covering all modes of relaxation experienced by the chain, flexibility of the chain, or chains of long lengths.

Here we monitor the transient behavior of various chains to provide scaling laws that are a function of the chain's length, stiffness, and time. Because it is time consuming to study chains of long length over extended time periods, understanding the scaling behavior of the property will prove useful. The properties of interest here are the chain lengths, normal stresses, and birefringence. Not only are we interested in the properties at equilibrium but how the chain undergoes the conformation transition and the change in properties along the way to equilibrium.

3.2.1 Dynamics and Time Scales

The relaxation process is governed by the chain's various length scales; short, intermediate and long. An understanding of the semiflexible chain's relaxation mechanism can be seen by looking at the forces involved in the three different

time periods. Initially, because the chain is straight, bending forces, if present, are negligible and the tension force on each bead is seen to scale as $T \sim N^2$. Hence, at short-times $t \ll N^{-2}$, both flexible chains (E=0) and stiff chains ($E > N$) display a free transverse bead diffusion $d_\perp^2 \sim t$, due to the dominance of the transverse Brownian forces over the transverse tension forces $F_\perp^{ten} \ll F_\perp^{rand}$. At the transition time $\tau_{ten} \sim N^{-2}$, the tension forces and Brownian forces reach a balance. For flexible chains at intermediate-times $N^{-2} \ll t \ll N^2$, the tension forces dominate the dynamics and a quasi-steady equilibrium balance of the tension forces along the chain length is observed [15, 33]. Due to the presence of Brownian forces, a relaxation of the tension force is observed for flexible chains, when $t \sim N^2$ the tension becomes $T = O(1)$.

On the other hand, because of the added bending force, stiff chains exhibit two intermediate-time periods. At early intermediate-times $N^{-2} \ll t \ll N^4/E^3$, the chain is still almost straight; thus the longitudinal bending forces are negligible and the dominance of the longitudinal tension component is seen $F_\parallel^{bend} \ll F_\parallel^{ten}$; a behavior identical to flexible chains is observed. Only at the transition time of $\tau_{mid} \sim N^4/E^3$ does the tension force start to decrease due to the presence of both the Brownian and bending forces. The late intermediate-time period $N^4/E^3 \ll t \ll N^4/E$, exist when the chain stiffness begins to have a noticeable effect on the longitudinal relaxation process. The late intermediate-time period ends when the longest bending time scale for the polymer chain is reached $\tau_\perp \sim N^4/E$.

An influence of the chain length on the dominance of the tension and bending forces was also noticed. Long stiff chains, $N > (E/N)$, exhibit an early universal intermediate behavior due to their still straight chain configuration, while the late intermediate behavior was seen for all stiff chains due to the presence of the bending energy.

Finally, at long-times no behavior was noticed for stiff chains because the chains are already near equilibrium by the end of the intermediate-time period. In summary, the relaxation mechanism is governed by the relaxation of the tensions accumulated in the initial configuration. Table 3.1 shows an overview of the time scales for both flexible and semiflexible chains.

Table 3.1: Relaxation time scales for the bead-rod model

	$\tau_{rand} \sim \zeta b^2/k_B T$	unit time
$E = 0$	$\tau_{ten} \sim N^{-2}$	short-time
flexible	$\tau_{nmode} \sim N^2$	long-time
$E \geq N$	$\tau_{bend} \sim E^{-1}$	short-time
semiflexible	$\tau_{mid} \sim N^4/E^3$	early-intermediate time
	$\tau_{\perp} \sim N^4/E$	late-intermediate time

3.2.2 Configuration

Because single bead motion is affected only by the neighboring beads, a quick (a few time decades) relaxation of the bead is noticed; thus a clear understanding of the full chain configuration is not able to be seen over a large enough time period [19, 33]. We expand on previous studies by considering the transient behavior of the eigenvalues. Because the second and third eigenvalues show the same relaxation behavior, discussion is limited to the behavior of the second eigenvalue.

For completeness we review the behavior of flexible chains as presented by Dimitrakopoulos [15]. By looking at the unscaled relaxation behavior of the chain length, one can see the polymer chain stays aligned in the longitudinal direction well into late long times when rotation effects take place to incur a rapid relaxation. During short and intermediate-times, the chain expands in the transverse direction showing scaling laws of $R^2_{G,2} \sim t$ and $R^2_{G,2} \sim N^{-1/2}\, t^{3/4}$ respectively for the two time periods. In order to get the intermediate-time scaling behavior of $\Delta R^2_{G,1} \sim N t^{1/2}$, the reduction of the property with its zero time value $\Delta R^2_{G,1} = R^2_{G,1}(0) - R^2_{G,1}(t)$, is scaled with N^2 (the scaling at the end of the intermediate-time) while the first normal mode relaxation is used (i.e., the long-time relaxation scaling) $\tau_{nmode} = \tau_{rand} \left[12 \sin^2(\frac{\pi}{2(N+1)}) \right]^{-1}$, to get an overlap of the curves at intermediate-times. Chain anisotropy is observed by the differences in the transverse intermediate-time behavior of $R^2_{G,2} \sim t^{3/4}$ and the longitudinal intermediate-time behavior of $R^2_{G,1} \sim t^{1/2}$. At long-times, the re-

duction of the property is taken with respect to its equilibrium value, such that $\delta R^2_{G,1} = R^2_{G,1}(t) - (R^2_{G,1})_{eq}$ where $(R^2_{G,1})_{eq} = 0.76(R^2_G)_{eq}$.

The intermediate longitudinal and transverse relaxations of an initially straight stiff chain are shown in figures 3.1 and 3.2. The short-time free bead diffusion is shown along with the scaling behavior for both the early and late intermediate-times. The early intermediate-time behavior of the chain's width $R^2_{G,2} \sim N^{-1/3}t^{5/6}$ is seen in figure 3.2a, while the longitudinal universal relaxation of $\Delta R^2_{G,1} \sim Nt^{1/2}$, is seen again in the early-time behavior in figure 3.1a. The late intermediate-time behavior of the chain's length and width behavior can be seen in figures 3.1b and 3.2b. The dependence of the chain stiffness E is noticed during the late intermediate-time period, where the chain length is seen to grow as $\Delta R^2_{G,1} \sim N^2E^{-3/4}t^{1/4}$, see figure 3.1$b$, and the width increases as $R^2_{G,2} \sim E^{-1/4}t^{3/4}$, see figure 3.2$b$.

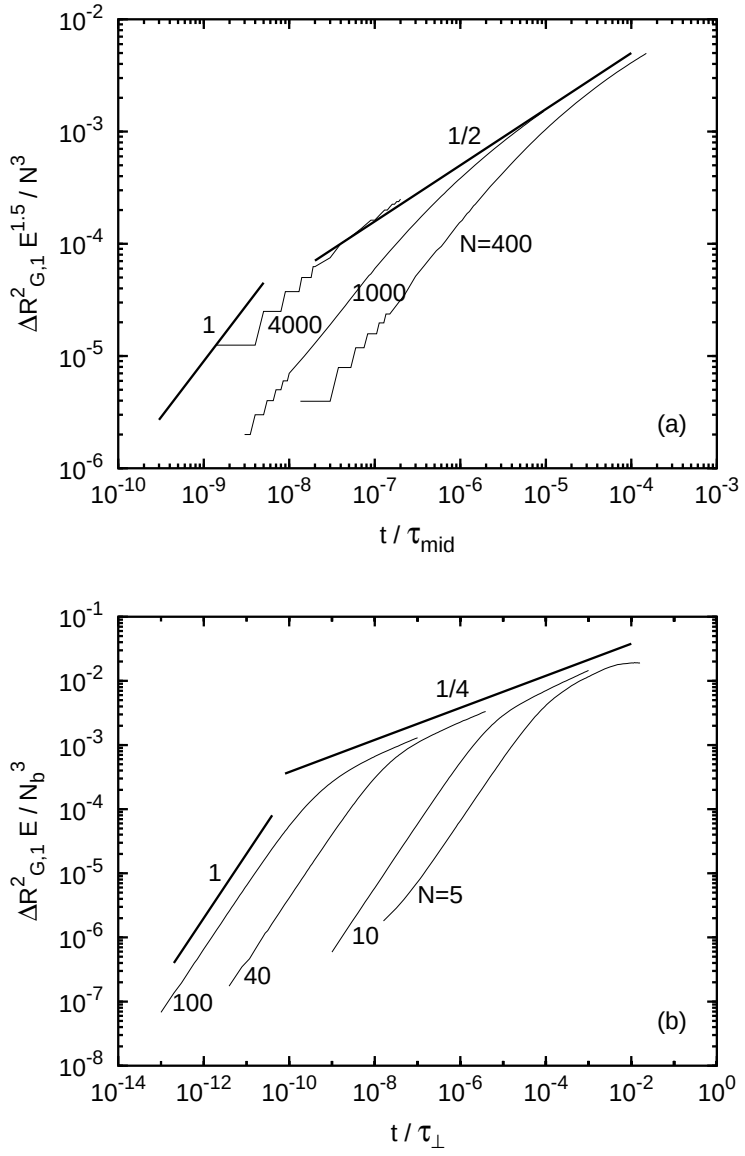

Figure 3.1: Scaling law for the relaxation of the chain's length for stiff polymer chains with $E/N = 10$ at (a) early intermediate-times and (b) late intermediate-times. The free diffusion at short-times is also shown.

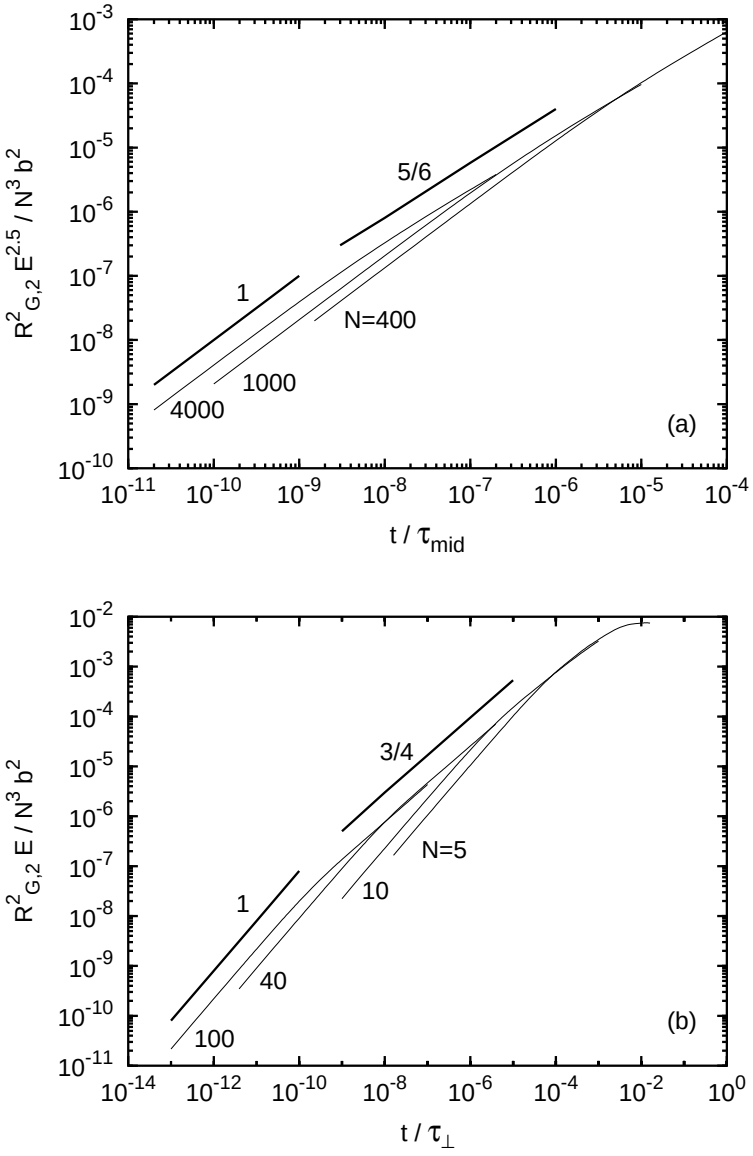

Figure 3.2: Scaling law for the relaxation of the chain's width for stiff polymer chains with $E/N = 10$ at (a) early intermediate-times and (b) late intermediate-times. The free diffusion at short-times is also shown.

3.2.3 Stress

As a straight chain configuration only normal stresses are present. The first normal stress component σ_{11}, is effected by the chain's tensions in the longitudinal direction, $\sigma_{11} \sim \sum T \sim R_{G,1} F_{\parallel}^{ten}$ while the the weaker stress σ_{22} is due to the transverse Brownian force. Through our earlier analysis on the polymer configuration and dynamics, we can now better understand the polymer stress relaxation behavior by recognizing the dependence of the stress on the longitudinal length component.

The flexible relaxation behavior of the two normal stress components can be found in reference [15]. Similar to the relaxation of the configuration, anisotropy in the stress is also noticed, $\sigma_{11} \sim t^{-1/2}$ while $\sigma_{22} \sim t^{-1/4}$, during the intermediate-time period.

Figure 3.3 displays the early and late intermediate behavior of $E/N = 10$ stiff chains. As expected, figure 3.3a shows the universal $\sigma_{11} \sim N^2 t^{-1/2}$ relaxation behavior observed for the flexible chains. At late intermediate-times a power law scaling of $\sigma_{11} \sim N^3 E^{-3/4} t^{-3/4}$ is noticed. Because there is no change in the polymer length until long times, the short and intermediate time stress relaxation behavior is affected only by the change in the transverse direction. Not until long times is there a rapid stress relaxation seen due to the relaxation of the chain length and corresponding tensions.

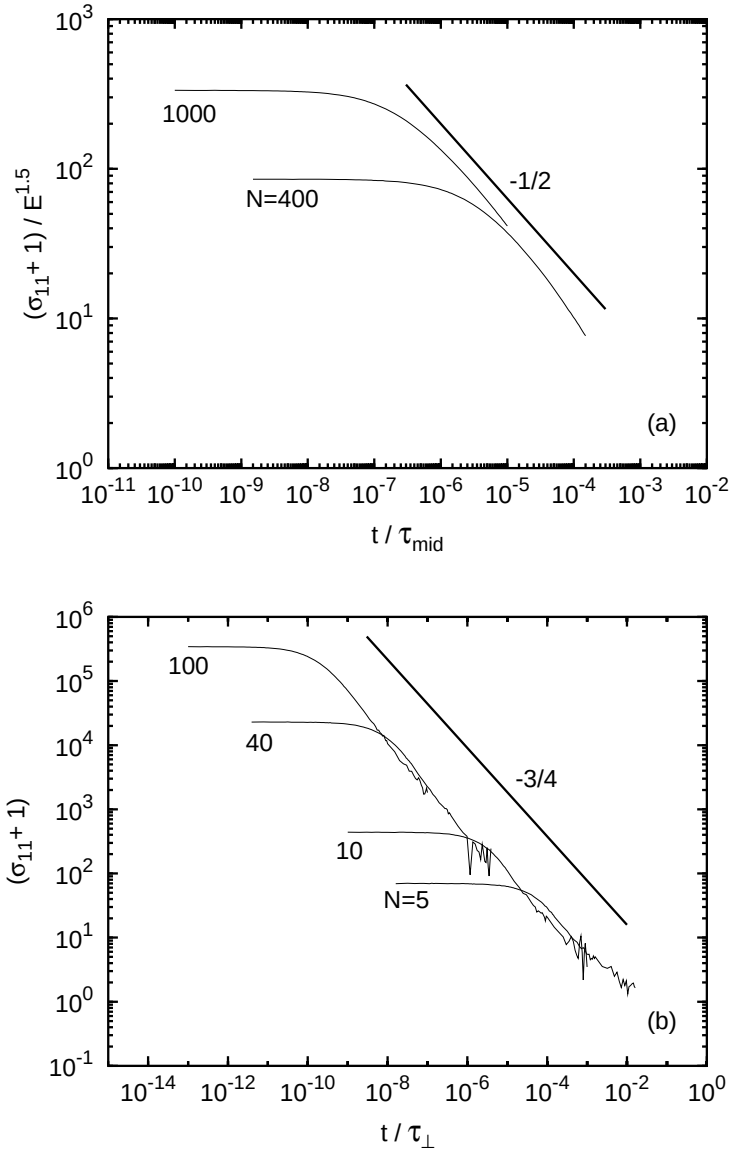

Figure 3.3: Scaling law for the relaxation of the chain's normal stress component σ_{11}, for stiff polymer chains with $E/N = 10$ at (a) early intermediate-times and (b) late intermediate-times.

3.2.4 Birefringence

Previous Brownian dynamics studies on birefringence relaxation have been limited to the long-time behavior and the index of refraction was indirectly studied through a linear stress-optic coefficient [19, 21].

We first examine the components of the refractive index tensor for polymer relaxation. By doing so, it was noticed, as seen in figure 3.4, that n_{12} has no distinct behavior and is much smaller in magnitude compared to the difference of the two normal components. Based on this analysis, n_{12} can be eliminated from Eq. (9) allowing birefringence to be simplified into

$$B \cong n_{11} - n_{22}. \tag{1}$$

At equilibrium the birefringence of the chain is zero; consequently, the two normal components are equal in value $(n_{11})_{eq} = (n_{22})_{eq} = (n_{33})_{eq} = N/3$ as seen in figure 3.5.

Because of the linear birefringence relation described in Eq. (1), the refractive indices display the same scaling behavior as the birefringence. The flexible scaling behavior of both the refraction indices and birefringence relaxation can be seen in figures 3.6, 3.7 and 3.8.

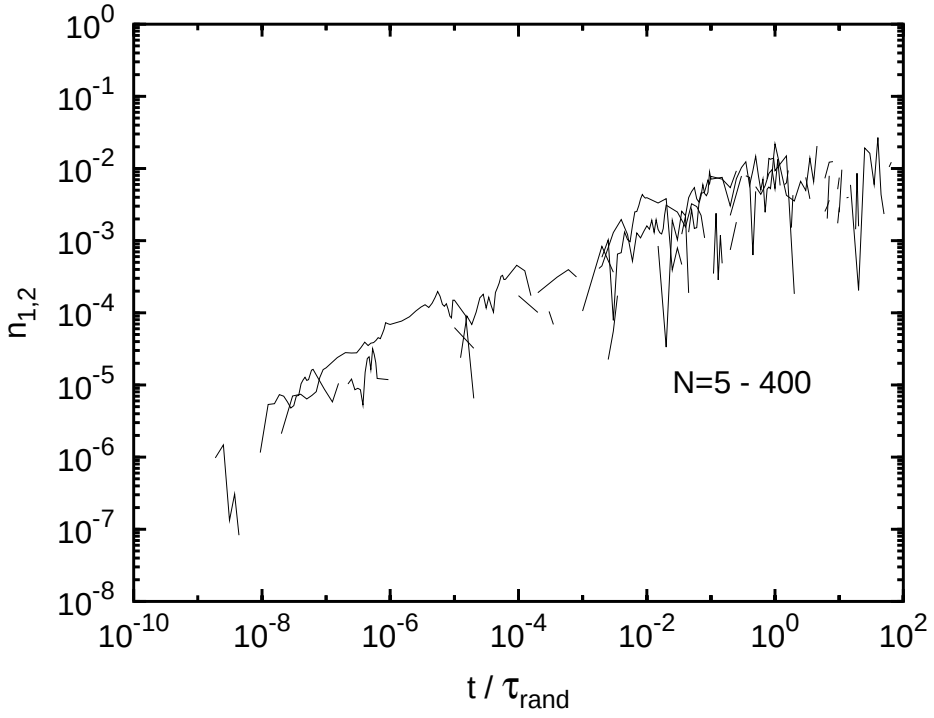

Figure 3.4: Relaxation of the refractive index component n_{12}.

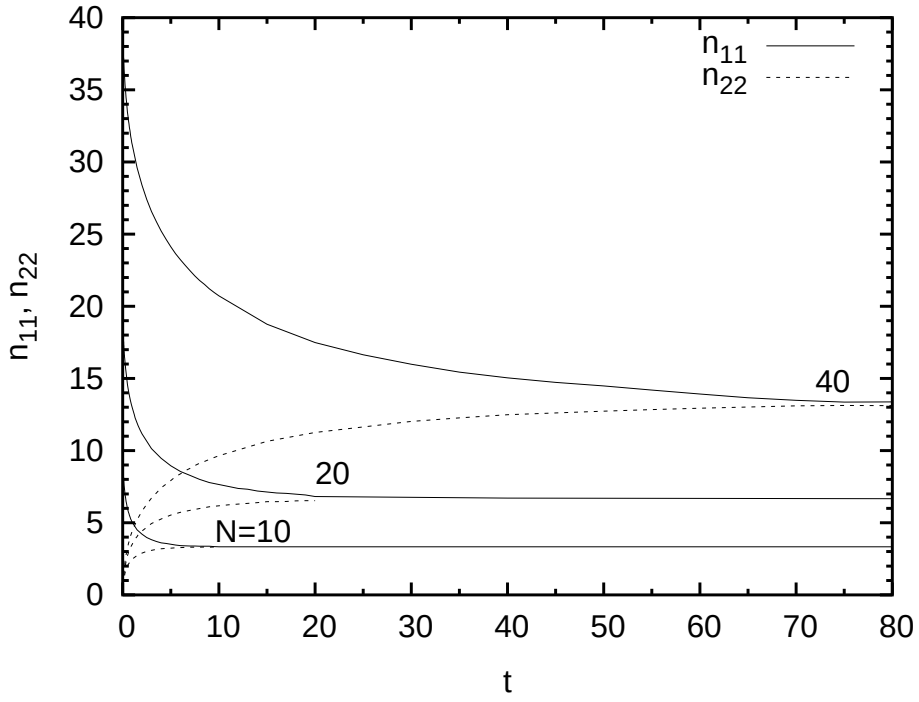

Figure 3.5: Unscaled relaxation behavior of the normal refractive index components n_{11}, n_{22}.

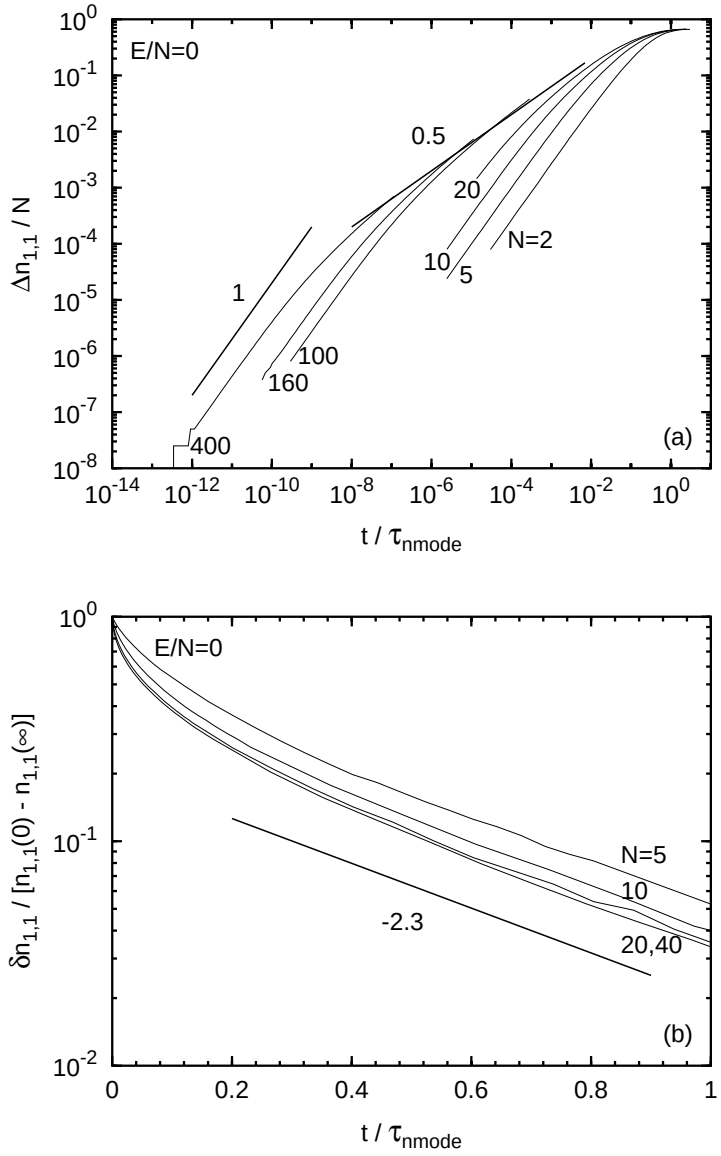

Figure 3.6: Scaling law for the relaxation of the reduction of the first index of refraction for flexible polymer chains at (a) intermediate-times and (b) long-times. The free diffusion at short-times is also shown.

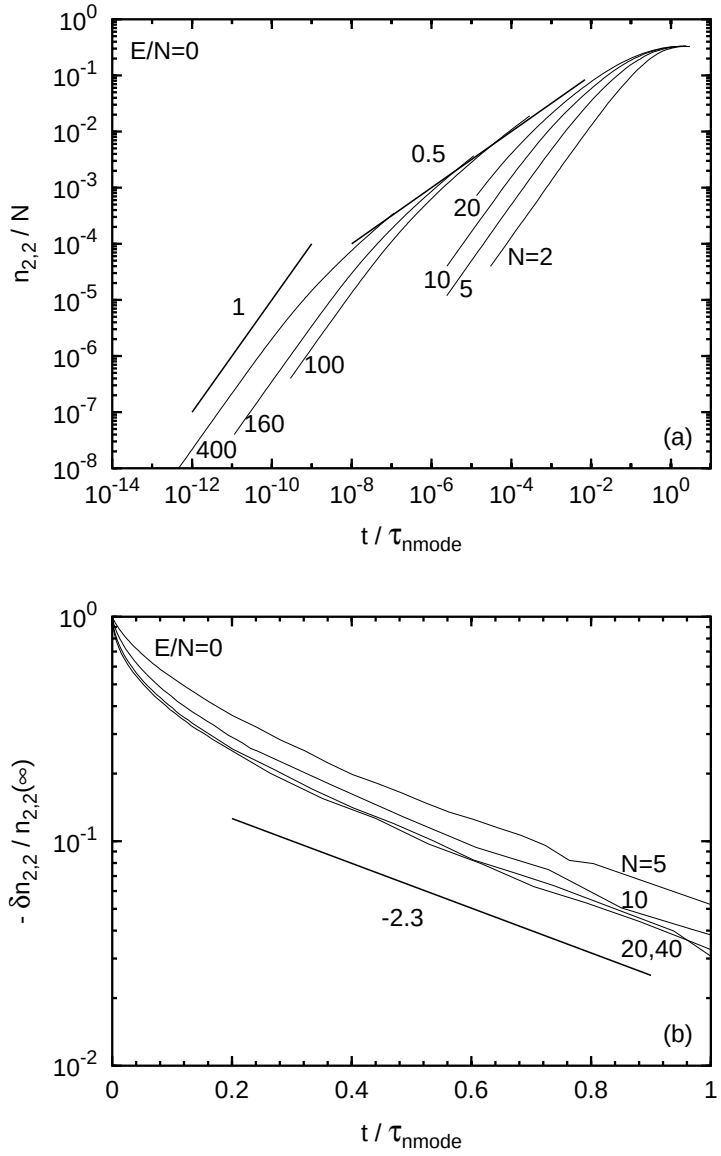

Figure 3.7: Scaling law for the relaxation of the second index of refraction for flexible polymer chains at (a) intermediate-times and (b) long-times. The free diffusion at short-times is also shown.

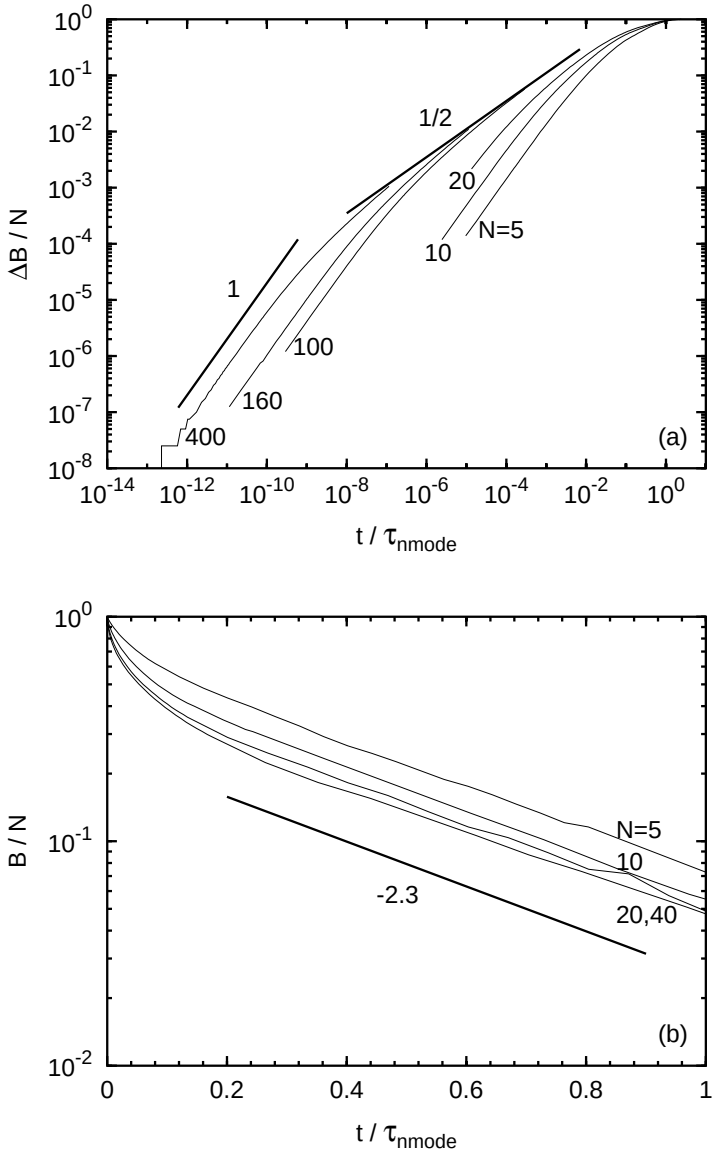

Figure 3.8: Scaling law for the relaxation of the birefringence reduction for flexible polymer chains at (a) intermediate-times and (b) long-times. The free diffusion at short-times is also shown.

The optical evolution for flexible chains shows free diffusion at short-times, an intermediate-time behavior of $B \sim t^{1/2}$ in figure 3.8a, and a long-time exponential decay of $B \sim N\, exp(-2.3\, t/\tau_{rouse})$ in figure 3.8b. The long time decay also matches the long-time behavior originally found by Doyle *et al.* [19].

Due to the similar behavior of the refractive indices with birefringence, the semiflexible behavior of only birefringence is shown in figures 3.9 and 3.10. As seen in figure 3.9, both short and long stiff chains, due to the free diffusion, have the same linear scaling of $\Delta B \sim Nt$ at short-times. As expected, the evolution for stiff chains reveals the same early universal law of $B \sim t^{1/2}$, followed by a late power law of $\Delta B \sim NE^{-3/4}t^{1/4}$, as shown in figure 3.10.

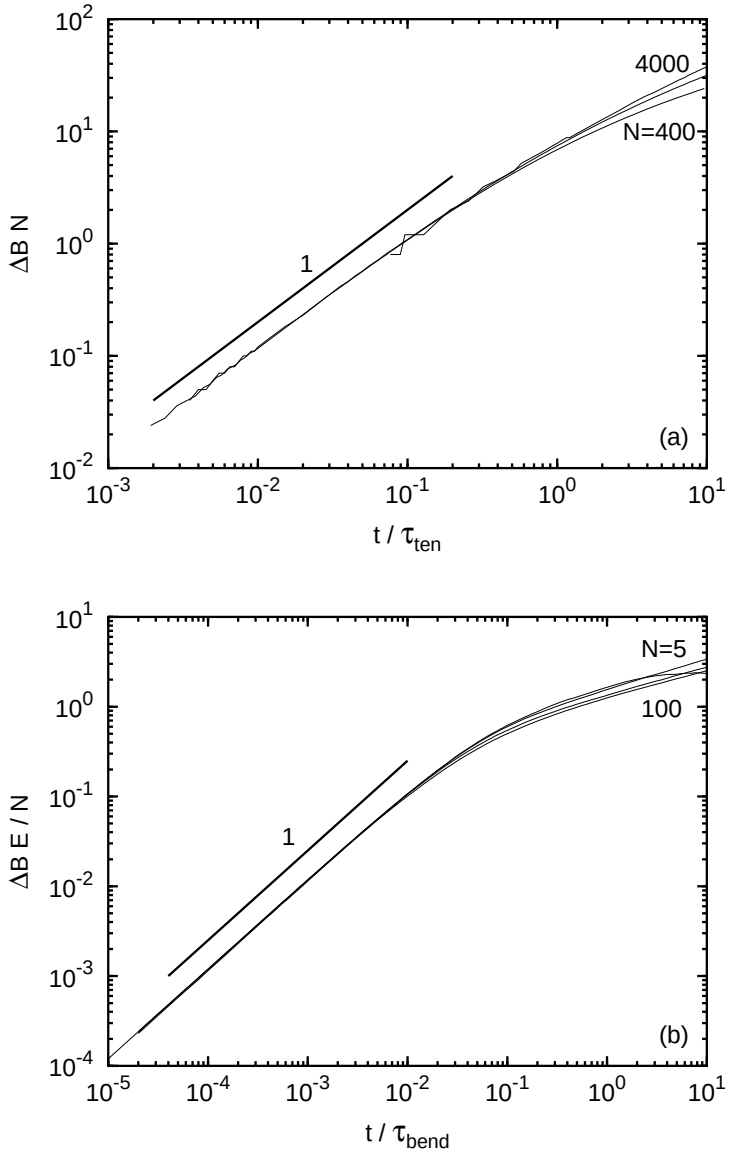

Figure 3.9: The short-time linear scaling law for the relaxation of the birefringence reduction of (a) long and (b) short stiff polymer chains with $E/N = 10$. Note that $\Delta B = B(0) - B(t) = N - B(t)$.

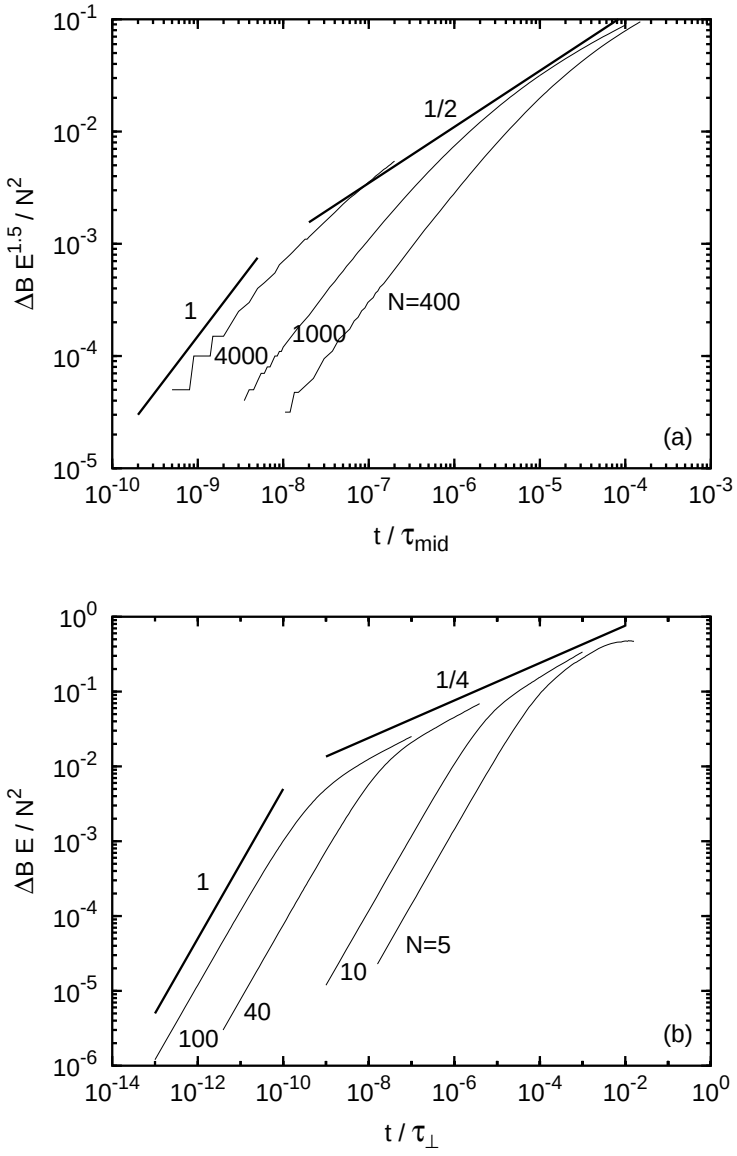

Figure 3.10: Scaling law for the relaxation of the birefringence reduction for stiff polymer chains with $E/N = 10$ at (a) early intermediate-times and (b) late intermediate-times. The free diffusion at short-times is also shown.

As the chain relaxes toward its equilibrium shape, the decay of both normal refractive index components are seen to be related to the chain's longitudinal relaxation. Even though the second normal component is a function of the perpendicular chain orientation $n_{22} = \sum d_{\perp}^2$, as mentioned earlier due to fixed bond lengths, the link width is a function of the chain's length $R_{\parallel}$, so both the normal index components are a property of the chain length. Thus, the optical properties can be defined as a function of the chain's longitudinal length such that $\Delta B \sim \Delta R_{G,1}^2/N$. A summary of the power-law behaviors found for the three properties is seen in table 3.2.

Table 3.2: Relaxation behavior of the bead-rod model for semiflexible chains

length	$\Delta R_{G,1}^2 \sim N t^{1/2}$	early-intermediate time
	$\Delta R_{G,1}^2 \sim N^2 E^{-3/4} t^{1/4}$	late-intermediate time
width	$R_{G,2}^2 \sim N^{-1/3} t^{5/6}$	early-intermediate time
	$R_{G,2}^2 \sim E^{-1/4} t^{3/4}$	late-intermediate time
stress	$\sigma_{11} \sim N^2 t^{-1/2}$	early-intermediate time
	$\sigma_{11} \sim N^3 E^{-3/4} t^{-3/4}$	late-intermediate time
birefringence	$\Delta B \sim t^{1/2}$	early-intermediate time
	$\Delta B \sim N E^{-3/4} t^{1/4}$	late-intermediate time

A relationship between the refractive index tensor and the stress tensor can be found through the stress-optic law $\boldsymbol{n} = C\boldsymbol{\sigma}$, where C is the stress-optic coefficient [24]. From this proportionality, knowing the birefringence of the material allows for understanding of the stresses present. The constant coefficient C, has been found to be independent of molecular weight but dependent on the solvent, where after a limit is reached the polymer concentration has no effect on the constant [24]. Experiments and simulations have shown the validity of this linear relation for weak flow rates only. Doyle *et al.* studied the law for the relaxation of flexible chains and concluded that the coefficient is constant only at long-times [19]. A more general relation between stress and birefringence was recently seen in the work of Ghosh *et al.* [27]. This relation however, is only valid for the intermediate and long-time relaxation of flexible chains.

Based on our results on the relaxation behavior of the polymer stress and index of refraction and their dependence on $\Delta R_{G,1}$, we have formulated a generalized nonlinear stress-optic law

$$\sigma_{11} \sim N^2 \frac{d(B(0) - B(t))}{dt}. \tag{2}$$

This law is valid for all time periods and for any chain stiffness. Figure 3.11 displays the stress-optic law for stiff chains. The chains show that with time the ratio of actual stress to stress predicted by Eq. (2) is constant. Noise in the data is

due to the calculation of the derivative $d(B(0)-B(t))/dt$. Also, for long chains we were able to see behavior independent of N with the ratio remaining at a constant value of ~ 0.02.

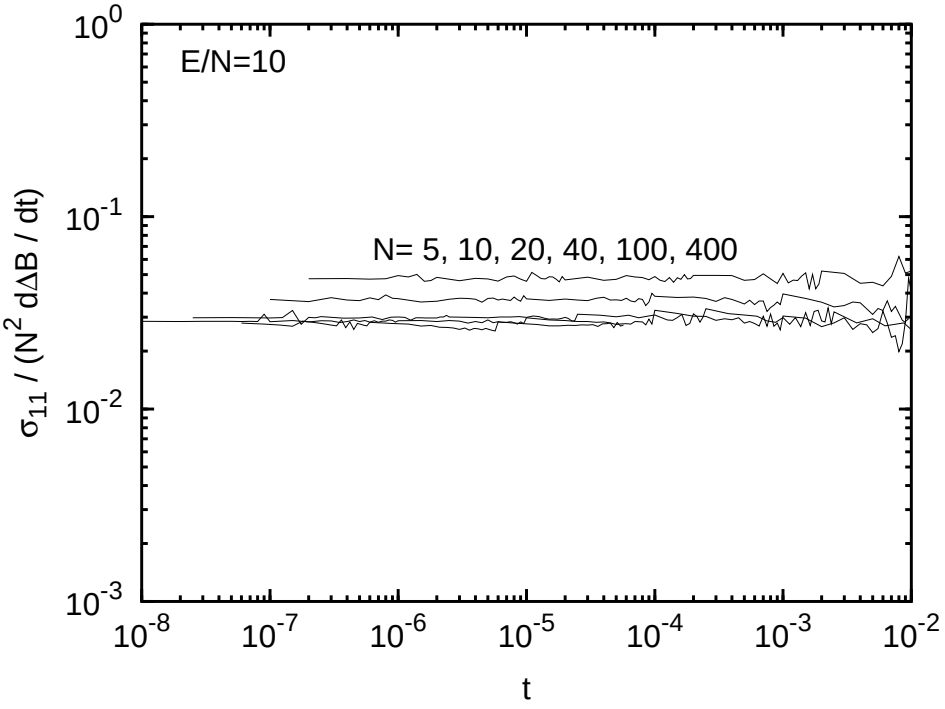

Figure 3.11: Stress-optic law for stiff polymer chains with $E/N = 10$.

Chapter 4

Relaxation of a Worm-Like Chain

We continue our single molecule study by examining the relaxation dynamics of the worm-like bead-spring model. Even though the bead-rod model has been shown to model flexible polymer behavior such as polystyrene molecules, the force-extension curve of DNA has been well described by the WLC model [8]. In this model the bonds of the polymer are no longer rigid rods as in the bead-rod model but are represented as entropic springs accounting for the chain's elastic nature.

The appeal of polymers towards biological and industrial purposes are endless. The ability to predict the dynamics of biological and synthetic chains through computational modeling will be of great value. Towards this goal, we investigate the relaxation dynamics of the worm-like chain model. Through parallel computer resources, we try to capture and understand the polymer's properties missing in previous studies.

4.1 Introduction

One of the first attempts to model the bead-spring model towards the properties of DNA was done by Bustamante *et al.* [8]. The force extension study showed how DNA approaches its contour length with an inverse square-root dependence on the force. This model has been proven to successfully describe the force-extension behavior of DNA molecules. The force-extension measurements were further examined by Bouchiat *et al.* [7]. Here the persistence length was predicted for DNA molecules at low and high extension and found to be independent of the stretching force.

Ladoux and Doyle [41] studied and compared the behavior of a tethered WLC chain to a freely jointed chain. Under shear flow the effects of extension was predicted through theory, simulations, and experiment. A scaling analysis showed that the freely jointed chain is more easily extended than the WLC. This difference can be explained by looking at the spring force laws of the two models. The scaling laws were confirmed through Brownian dynamics simulations and fluorescence microscopy experiments on $\lambda - phage$ DNA chains. The experimental relaxation time was also measured by stopping the shear flow and allowing the molecules to come to equilibrium. The authors determined the following relaxation times, $\tau = 0.45\,s$, $\tau = 1.45\,s$, and $\tau = 2.56\,s$ for a λ, 2λ, and 3λ length DNA molecules, respectively. Experimental extension data for the three tethered molecules were plotted against the scaling laws for the two chain models and agreement with the

WLC scaling was noted. The results closely followed the extension rate predicted by the WLC. Hydrodynamic interactions were neglected.

Jendrejack *et al.* [34] extended the WLC study by looking into the effects of hydrodynamic interactions on the model. The authors show how the bead-spring model can be used to correctly predict the stretch behavior of chains up to six times longer ($N_s = 60, L_c = 126\mu m$) by proportionally increasing the number of springs in the WLC model. The longest relaxation time of the WLC model is described as

$$\lambda = \frac{\zeta b_k^2 N_{k,s}}{24 k_B T \sin^2(\frac{\pi}{2N_b})} \tag{1}$$

where $N_{k,s}$ represents the number of Kuhn steps per spring. The maximum spring length can then be described as $clen = b_k N_{k,s}$. The Brownian dynamics algorithm held the Kuhn length constant and accounted for both EV and HI. The behavior of longer chains was seen to be better predicted by the HI model.

A later work by Shaqfeh *et al.* [63] looked into the transient behavior of both the WLC and inverse Langevin spring chains following extensional flow. The effect of various flow rates was measured to determine the relaxation of the chains. As was seen earlier by Doyle *et al.* [21] for the bead-rod model, the authors saw a universal stress relaxation. After large deformation, under different strain rates, the stresses were seen to collapse onto a single curve. A difference in the stress decay of the two models was also noted. The WLC follows a power-law decay

of -0.69 while the freely-jointed chain follows the flexible -0.5 power-law decay predicted by earlier authors. Stress relaxation was measured directly through experiment and Brownian dynamics simulations.

The recent observations of Brownian dynamics simulations on the WLC model are limited. Studies using the spring model have focused more on the extension dynamics of the chain when placed under a linear flow field or subjected to force-extension tests. There is still much to be gained on the physics of semiflexible WLC chains.

4.2 Results and Discussion

Here we expand on our earlier relaxation study by shifting focus to the WLC bead-spring model. Via Brownian dynamics simulations we have captured the relaxation of chain length, width, stress, and spring force behavior.

In this model the polymer elastic force is represented by springs while the drag force is accounted for by the chain beads. The springs connecting the beads represent many Kuhn steps; therefore, making this model ideal for the study of long chains. To limit the maximum extension of the springs a nonlinear spring potential is added. Due to possible large fluctuations of the chain length, care must be taken to ensure that the spring length does not exceed the maximum bond length. Setting a restriction of $dmag < clen$ allows for the connecting vector to not exceed the maximum allowed spring extension. If the rate of stretching by a single spring is faster than the chain stretching, then the bead-spring model is no longer an appropriate representation of the polymer.

The mechanics of this model is based on the following spring law first recognized by Marko and Siggia [47]

$$\mathbf{F}_i = \frac{Hd_i}{6dmag_i}\left[\frac{1}{\left(1-\frac{dmag_i}{clen_i}\right)^2} - 1 + \frac{4dmag_i}{clen_i}\right]. \tag{2}$$

where H, the spring constant, is a function of the Kuhn length. Since our interest is on semiflexible chains we set $b_k = 0.005$. To realistically model the chain and avoid over-stretching we set the initial conformation to 99% extension and reject conformations where the maximum extension is exceeded. The number of rejection steps is dependent on how large the adopted time step is. A large time step would result in a large bead displacement, thereby leading to a very large and unrealistic spring force. The size of the time step used in the simulations was dependent on the Kuhn length, spring extension, and the chain length. An inverse relationship with chain length was noticed, such that the smaller the length the smaller the time step needed. Consequently, greater computational time was required. Due to this drawback our results are limited to chains of up to 40 springs; however, our results cover several time decades. For a chain of 40 springs, a time step of 10^{-9} was used and studied at least 8 time decades to capture most of the chain's relaxation behavior. The simulations used 3200 independent realizations.

The unscaled relaxation behavior for the chain length is seen in figure 4.1. Similar to the bead-rod relaxation, we see a rapid longitudinal relaxation occurring late into the intermediate times. The short-time constant behavior of the length, coincides with the chain going through an initial relaxation in the transverse direction. The effect of chain length shows that the longer the chain the more time is needed for it to relax to its equilibrium state. The increase in bonds increases the competition between the Brownian force and the spring force delaying the

path back to equilibrium. Because the chains are not fully extended one can notice the initial value of the chain length is slightly smaller than the expected $0.1N^2$ value for a fully-extended chain. When compared to the long-time behavior of our relaxation study on flexible bead-rod chains, we see agreement.

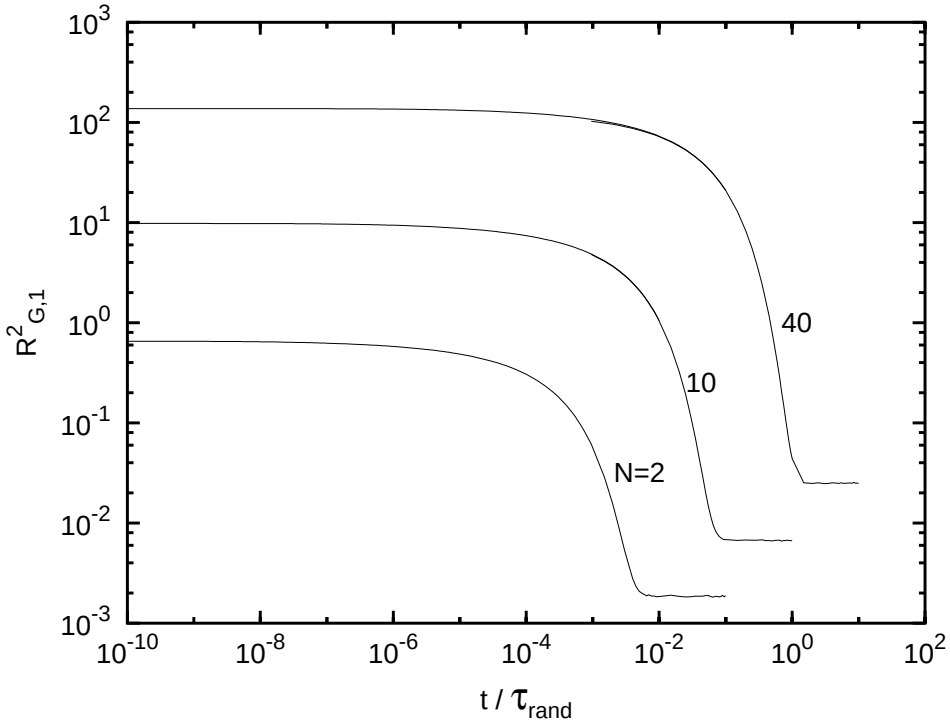

Figure 4.1: Unscaled chain length for N=2-40 of a WLC with $b_k = 0.005$.

The short-time length and width relaxation can be seen in figures 4.2(a) and 4.3(a) respectively. The transverse fluctuations give rise to a short-time free diffusion. This behavior, driven by Brownian motion, agrees with the predictions of the bead-rod model for short-time relaxation behavior. The single bead time scale of τ_{rand} accounts for the Kuhn length in the relaxation scaling.

During the early stages of stress relaxation we find the first normal component of stress scaling as high as Nb_k^{-2}. As shown in figure 4.4(a), the initial stress is proportional to N. Because of the inverse relationship with the Kuhn length, the stress of the nearly extended chain is seen to be large in value. The high growth in stress at the nearly extended state can be attributed to a loss of entropic freedom in the WLC. Figure 4.5(a) shows the relaxation behavior of the second normal stress component. We see an initial stress on the order of $N - 1$.

Furthermore, we have predicted the short-time spring force behavior for the three chain lengths of interest. The direct effect of the spring force is seen in figure 4.6. Initially the tension is as high as 10^6 and then relaxes down to an order of $\approx 10^3$ within 6 decades. We see at both zero-time and long-time that the spring force is independent of chain length. At extension and equilibrium the spring force is dependent only on the Kuhn length. The intermediate relaxation of the spring force as a function of length can also be seen.

The longest relaxation time of the WLC model described in Eq (1) has been simplified to:

$$\lambda = \frac{b_k}{24 \sin^2(\frac{\pi}{2N_b})} \tag{3}$$

for our model parameters. This time scale can then be used to predict the intermediate-time behavior of the chains. We show such behavior in figures 4.2(b), 4.3(b), and figure 4.4(b). At intermediate-times the chain length scales as

$$R^2_{G,1}(0) - R^2_{G,1}(t) = \Delta R^2_{G,1} \sim t^{0.35}, \tag{4}$$

while the width shows the same short-time free diffusion behavior. The continuous growth seen for the chain width is attributed to the beads being connected by entropic springs. The intermediate stress behavior predicts the following scaling

$$\sigma_{11} \sim t^{-0.69}. \tag{5}$$

This power law is in agreement with the recent findings of Shaqfeh *et al.* [63]. Finally, in examining the second normal stress component, seen in figure 4.5(b), we see a slower power law decay at the rate of 0.25, noticeable for the longer chains.

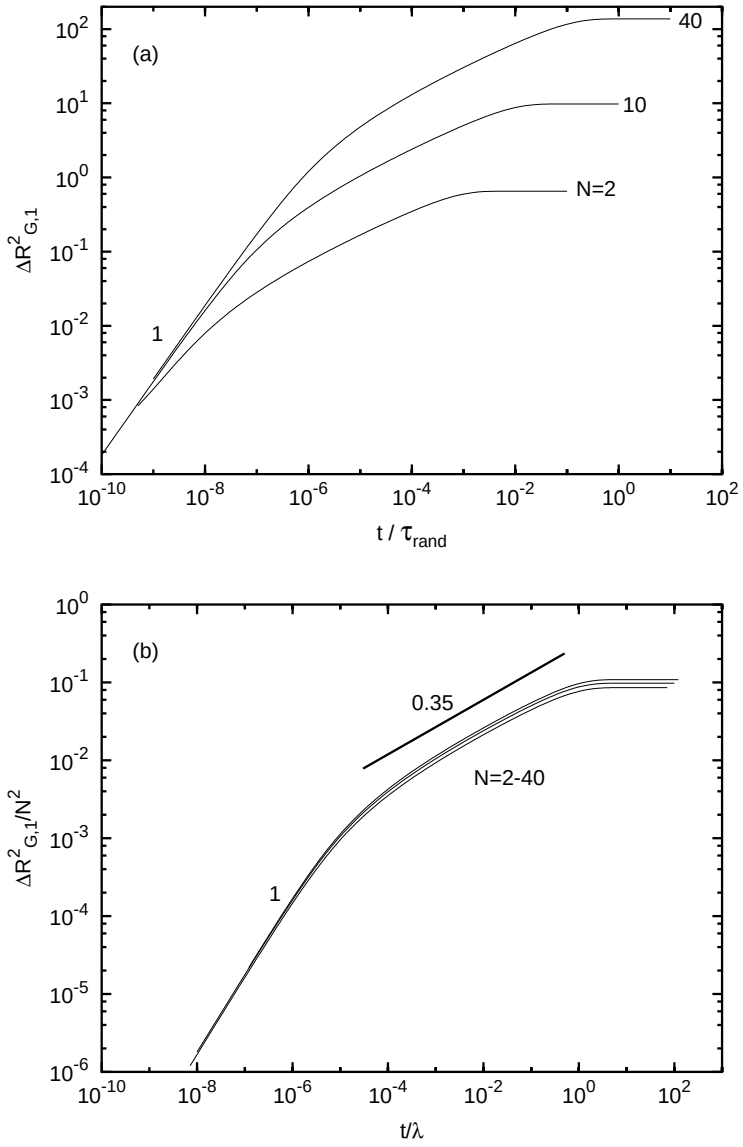

Figure 4.2: Scaling law for the relaxation of the chain's length for WLC with $b_k = 0.005$ at (a) short and (b) intermediate-times. Note that $\Delta R^2_{G,1} = R^2_{G,1}(0) - R^2_{G,1}(t)$.

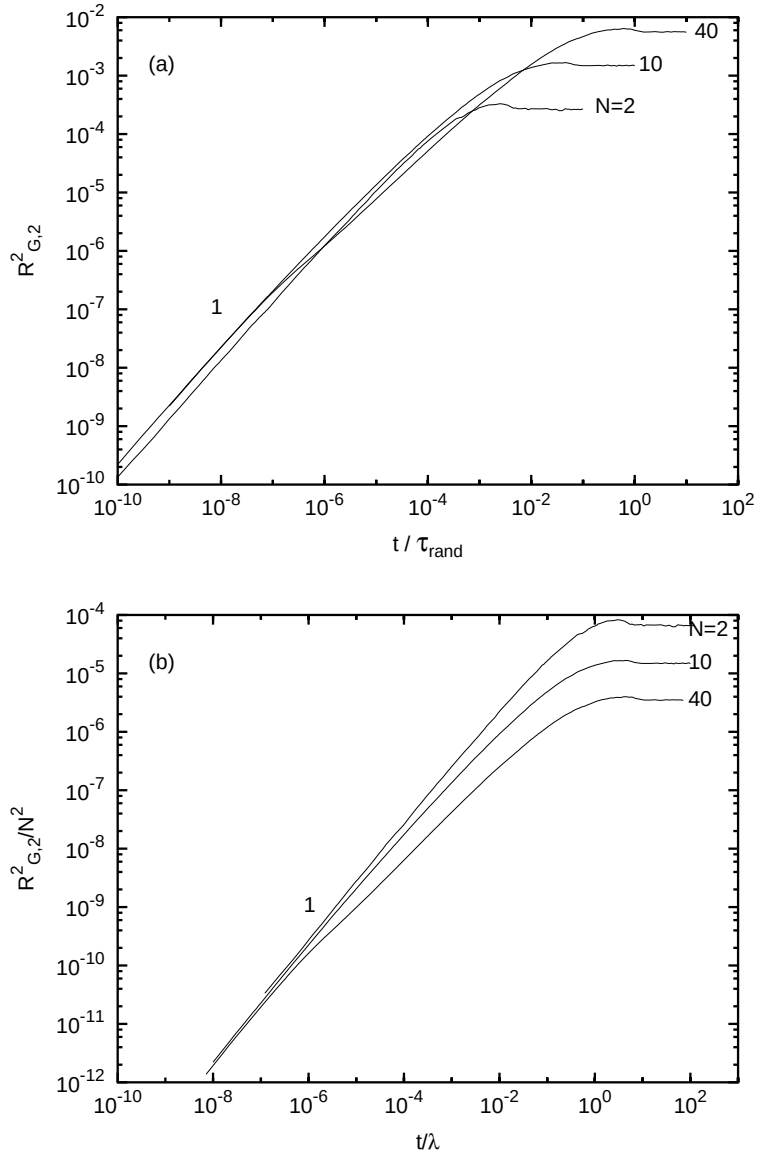

Figure 4.3: Scaling law for the relaxation of the chain's width for WLC with $b_k = 0.005$ at (a) short and (b) intermediate-times.

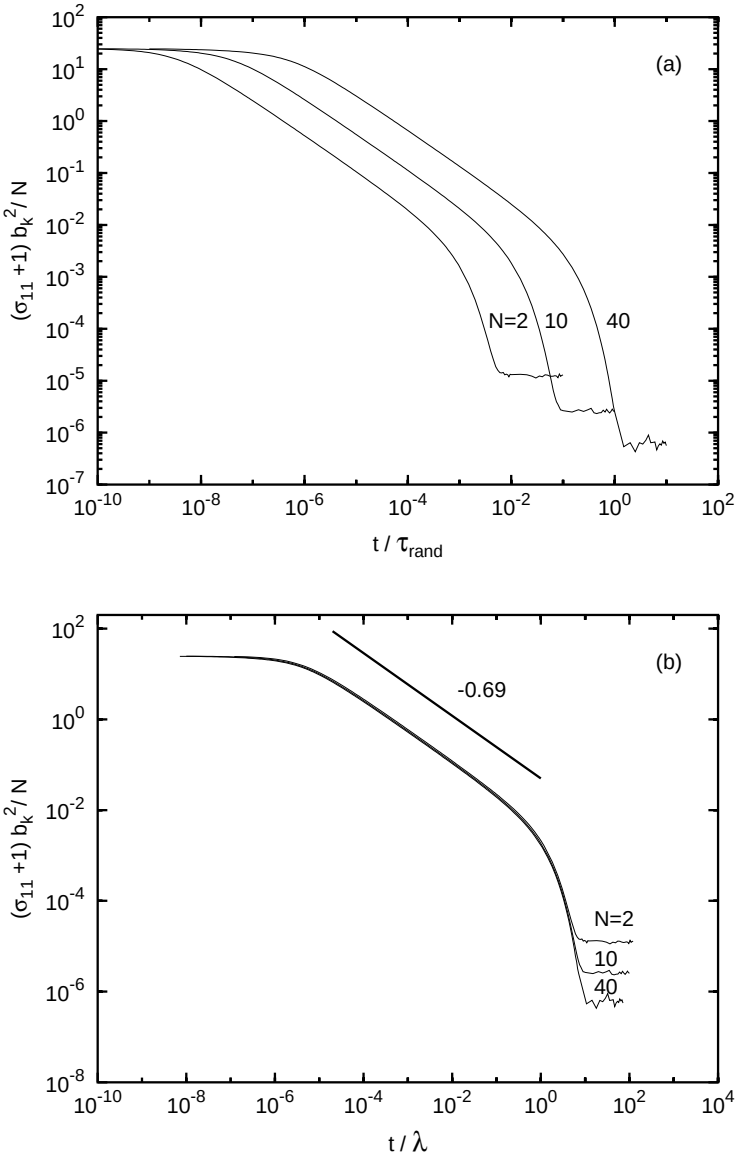

Figure 4.4: Scaling law for the relaxation of the chain's first normal stress σ_{11} for WLC with $b_k = 0.005$ at (a) short and (b) intermediate-times.

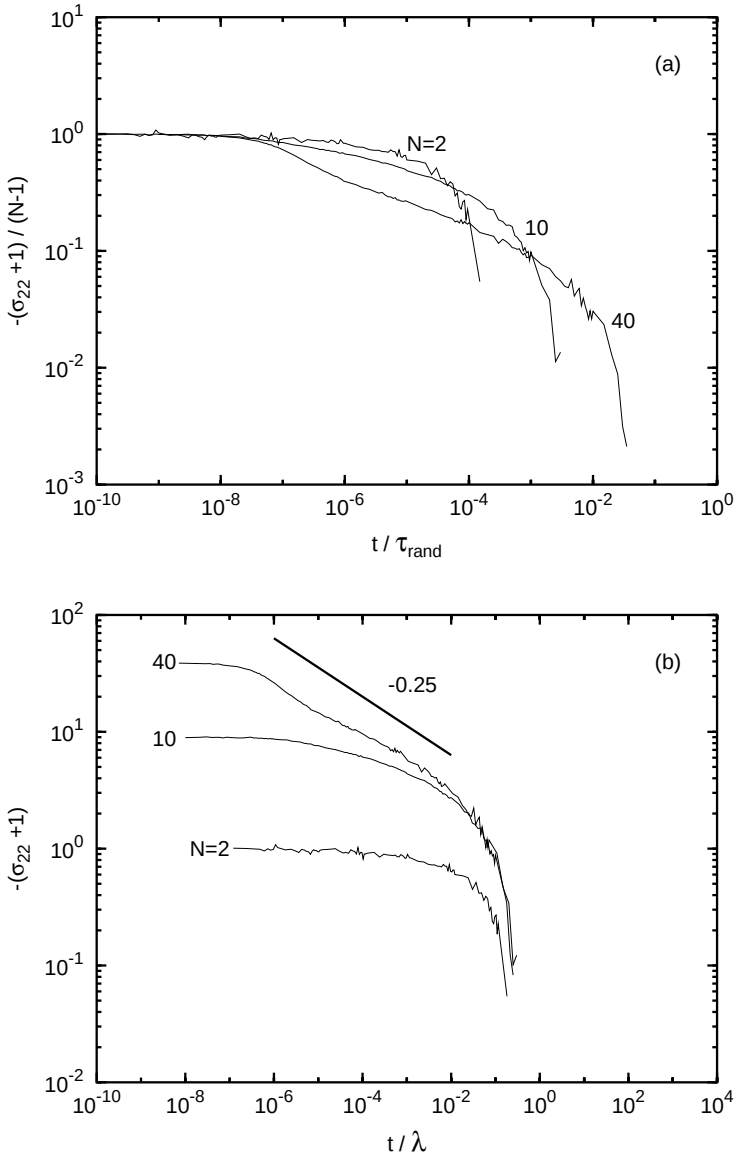

Figure 4.5: Scaling law for the relaxation of the chain's second normal stress σ_{22} for WLC with $b_k = 0.005$ at (a) short and (b) intermediate-times.

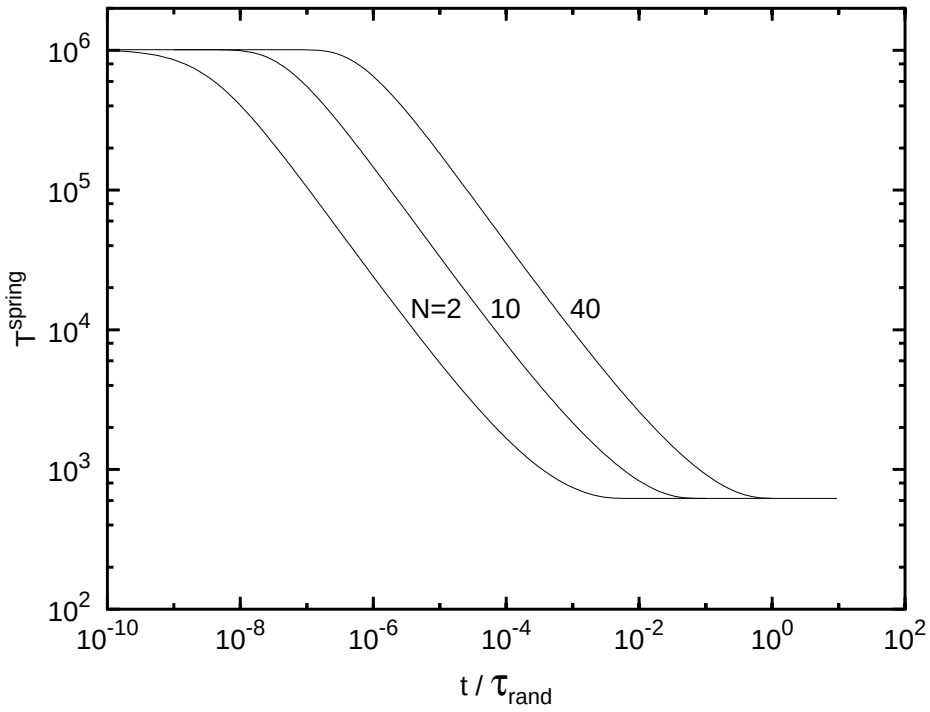

Figure 4.6: Short-time relaxation of the spring tension for WLC with $b_k = 0.005$.

The effect of the Kuhn length on a constant chain length of $N = 10$ was also studied. To avoid large computational costs, we first examine the influence of b_k on chains with an extension of 50%. The three lengths of interest were $b_k = 0.001$, $b_k = 0.005$, and $b_k = 0.05$. As can be seen in figure 4.7 the zero-time value of the chain length is independent of the Kuhn length and only dependent on the percentage of extension. We see the initial length of a 50% extended $N = 10$ WLC is ≈ 2.5. Not until late into the short-times is the effect of the rigidity noticed. As expected, a rapid decay of the most flexible chain, $b_k = 0.001$ is seen first. At long times we see the chains reaching full relaxation as evidenced by the end plateau. The effect of rigidity can be seen on the relaxation length, the higher the Kuhn length the more extended the final configuration is due to the presence of larger bending forces. Looking at the chain width in figure 4.8, we see again the zero-time value is free of chain rigidity. The rate of growth of the chain width is dependent on the stiffness, with the more rigid chain reaching a higher growth. Analysis of the stress behavior shows an initial inverse relationship with b_k, see figure 4.9. This inverse behavior can be explained by looking at the spring force law described in Eq (1), where we see the inverse dependence with b_k; recall that the spring constant is $H = \dfrac{3k_BT}{b_k}$. All chains equilibrate to the same end value. Finally, we show the relaxation behavior of the second normal stress component in figure 4.10. The relaxation is based on the degree of flexibility.

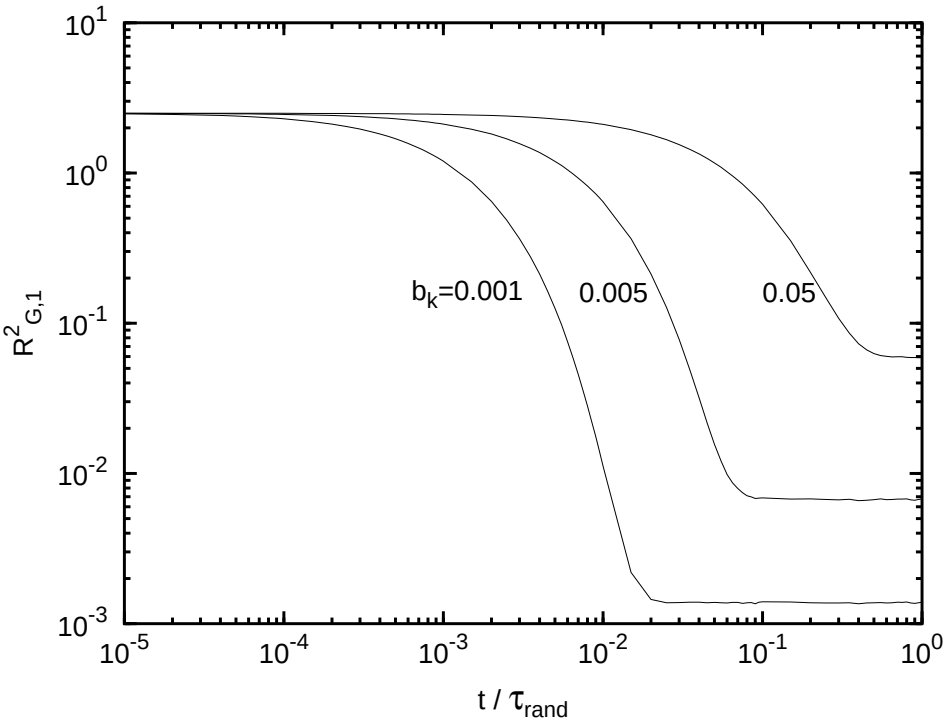

Figure 4.7: Chain length relaxation behavior of a N=10 WLC at various Kuhn lengths.

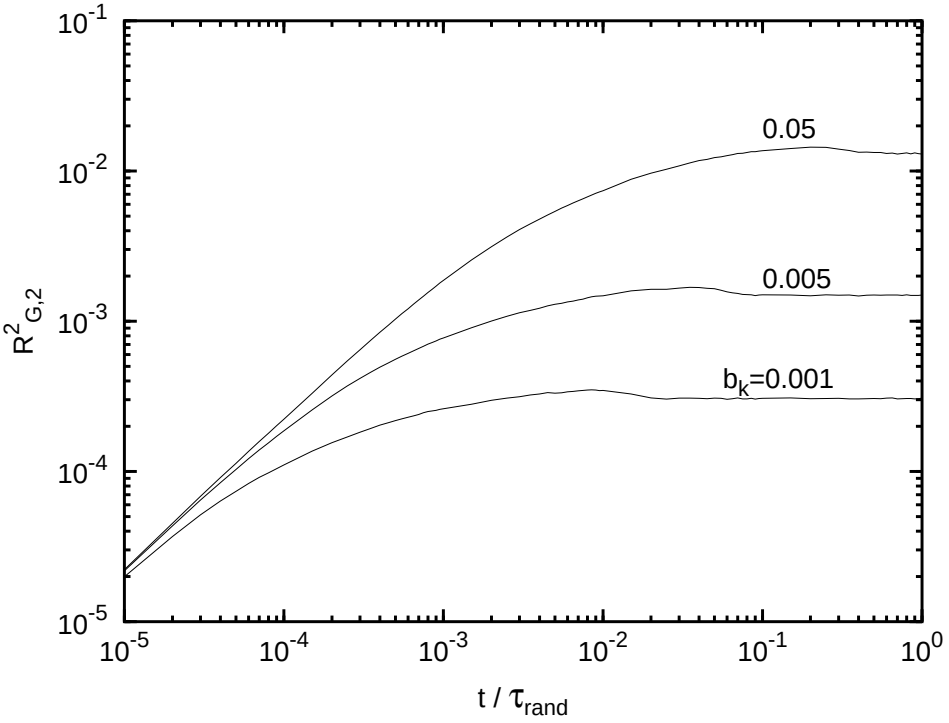

Figure 4.8: Chain width relaxation behavior of a N=10 WLC at various Kuhn lengths.

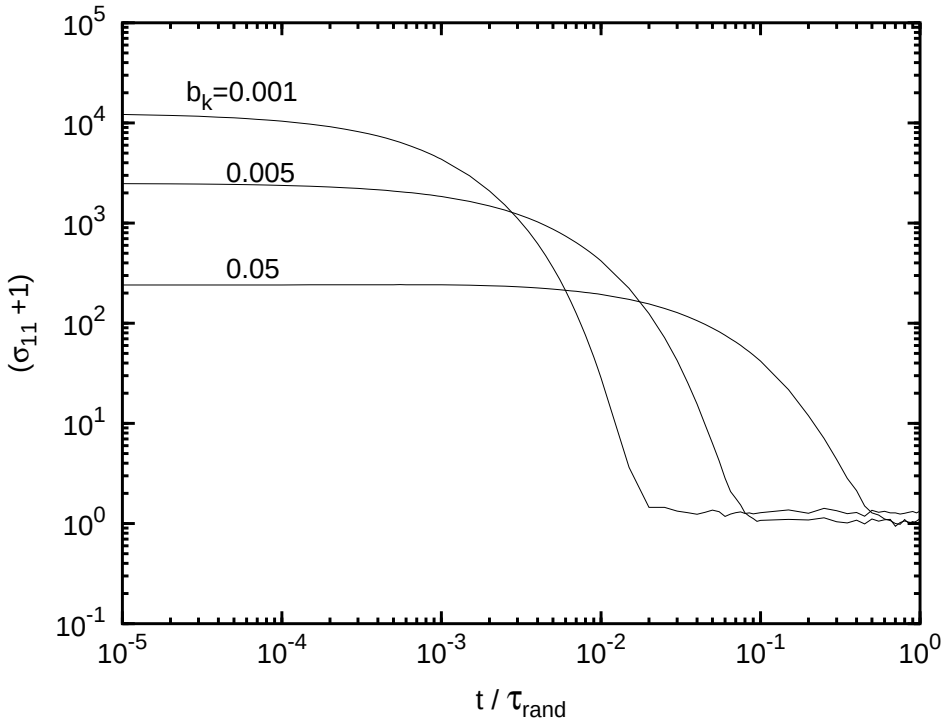

Figure 4.9: First normal stress relaxation behavior of a N=10 WLC at various Kuhn lengths.

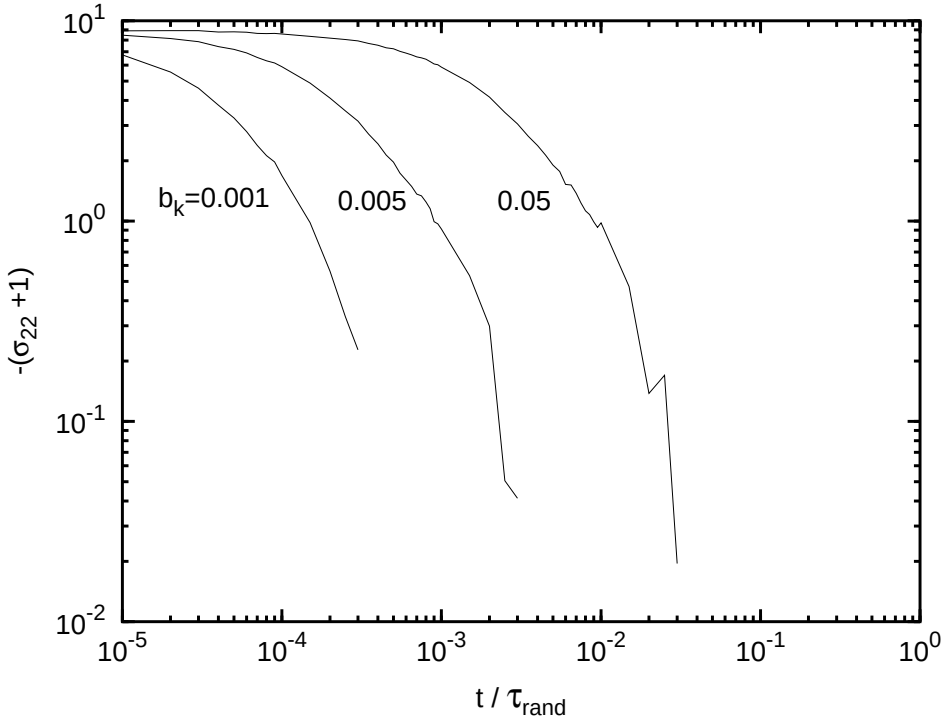

Figure 4.10: Second normal stress relaxation behavior of a N=10 WLC at various Kuhn lengths.

Chapter 5

Chain Stiffening

The focus of this chapter is to study and understand the dynamics a flexible chain undergoes when subjected to stiffening conditions. Studying the effect of chain flexibility on the macromolecule's properties is valuable towards further understanding the behavior of polymers experiencing a temperature, solvent, or structure change. This study is analogous to polymer systems changing conformations from that of a flexible coiled state to a rigid rod state due to the influence of surrounding conditions. The increase in stiffness is commonly experienced by nanoscale devices where the constrained polymer is subjected to rapid solution changes [59].

In this work, a method for the dynamic simulation of stiffened macromolecules is presented. The transient properties and conformations adopted by the chain have been studied extensively. We focus on understanding the transient dynamics of this coil-rod transition and its effect on the polymer properties.

5.1 Introduction

Past research has concentrated on polymers only at constant strength, however, with recent advances in technology, researchers have now been focusing on manipulating the rigidity of polymer chains to limit the chain bending. When subjected to external forces, such as strain or a change in solution conditions, such as an ionic strength increase, most polymer chains will stiffen. The increase in the chain persistence length, or chain Kuhn length, effects the polymer conformation and consequently its behavior in solution. The effect of stiffening polymer chains has been studied for both biopolymers and synthetic polymer systems.

Experimental studies on the ionic effects on the flexibility of single DNA molecules can be seen by Baumann *et al.* [5]. Through force extension studies Baumann *et al.* monitored chain elasticity as a function of both monovalent and multivalent cations. As monovalent salt concentration increased, from 1.86-586 mM, the chain persistence length decreased, from 96.3-45.1 nm. Multivalent cations such as Mg^{2+}, $putrescine^{2+}$, and $Co(NH_3)_6^{3+}$ were also studied, and the same inverse relationship was noticed.

Similar behavior has been observed for even concentrated solutions. Rouault [59], through Monte Carlo simulations monitored chain stiffening dynamics of a living polymer system. An interesting observation of this study was the effect the persistence length had on the chain contour length. An increase in the chain bending energy led to a decrease in the chain contour length. Upon reaching its

equilibrium rod-like state, further increase in bending energy resulted in a decrease in chain contour length.

Kemp *et al.* [36] studied the ordering of polymers as a function of temperature. In that work, the behavior of single molecules was investigated experimentally and computationally. Four distinct equilibrium configurations were revealed when amino acid monomers were subjected to a decrease in temperature. To reach the final stiff state, the flexible chain transitioned from a collapsed globular state, noticed by a decrease in R_g^2, to a flexible helical state where an increase in the chain size is noticed, to a final rod state. The protein organized itself at a given temperature such that its free energy was at a minimum, obeying thermodynamic laws.

Kinetic studies can be seen by Nisoli *et al.* [51] and Sakaue *et al.* [60]. Nisoli and co-workers followed the excitation kinetics of chains by the addition of various vinyl groups to the polymer backbone. The authors explore the flexibility effects based on the location and size of the side groups. The chain with alternating side groups, the most stiff chain, displayed the fastest kinetic decay to ground state. Relaxation was independent of size or location and only depended on the rigidity (i.e. how many side groups) of the chain. A similar study is seen by Sakaue *et al.* [60]. Here the coil-rod transition kinetics through chain nucleation and growth of a single semiflexible polymer chain was followed. Both the toroid and rod folding states were studied by observing the chain's internal energy and bond orientations.

The authors focused on comparing the folding and unfolding path of the polymer chain and concluded that a hysteresis exists.

Examples from the literature show knowledge on the polymer stiffening behavior has been gained through macroscopic measurements. A range of studies has been done in this area both experimentally and computationally to understand the dynamics, kinetics, and thermodynamics of the coil-rod transition. However, there is still much to be learned about the dynamic behavior and the physics involved in the stiffening process. Past experimental studies on this process have focused on the direct change to the chain persistence length, not the shape or property dynamics.

5.2 Results and Discussion

Existing stiffness studies, as seen from the review focus on the contour length effect, kinetics, and/or thermodynamics of the polymer chain. Focus on the expansion dynamics is rather limited and has not detailed the transient physics. The studies, also, have focused on semi-dilute to concentrated solutions. The objective here is to look at the effect on a single chain's physical properties as the shape transition from that of a coil to helix to rod state is made. By starting with a stiff chain forced into a coiled position and allowing it to extend over time, due to the bending and Brownian forces present, the effect of rigidity on the polymer chain properties can also be studied.

In our simulations, the time needed for the chain to reach the desired stiffness is rather small compared to the time the polymer takes to arrive at its final equilibrium shape; thus, we define the desired stiffness immediately at $t = 0$. At the end of the dynamic process, the chain equilibrates to its rod-like shape.

We have successfully modeled this interesting behavior. In figure 5.1 the initial coiled configuration for the N=100 chain is shown at time $t = 0$. Upon experiencing a bending energy of E/N=10, within a short period, the helical shape is assumed by time $t = 1$. This rearrangement of the beads can be attributed to a minimization in energy. Finally, the chain grows and equilibrates to reach its rigid rod structure as seen at time $t = 100$.

The evolution of the three eigenvalues for the $N = 100$ chain is seen in figure 5.2. Expansion and relaxation behavior for the three chain lengths has been predicted over 9 decades. Towards the end of the short-time we see a gradual increase in the two chain widths, signalling the growth of the helix. Upon reaching their maximum the two eigenvalues rapidly decrease causing the chain to grow in the 1-D direction; i.e., to become a rod-like polymer.

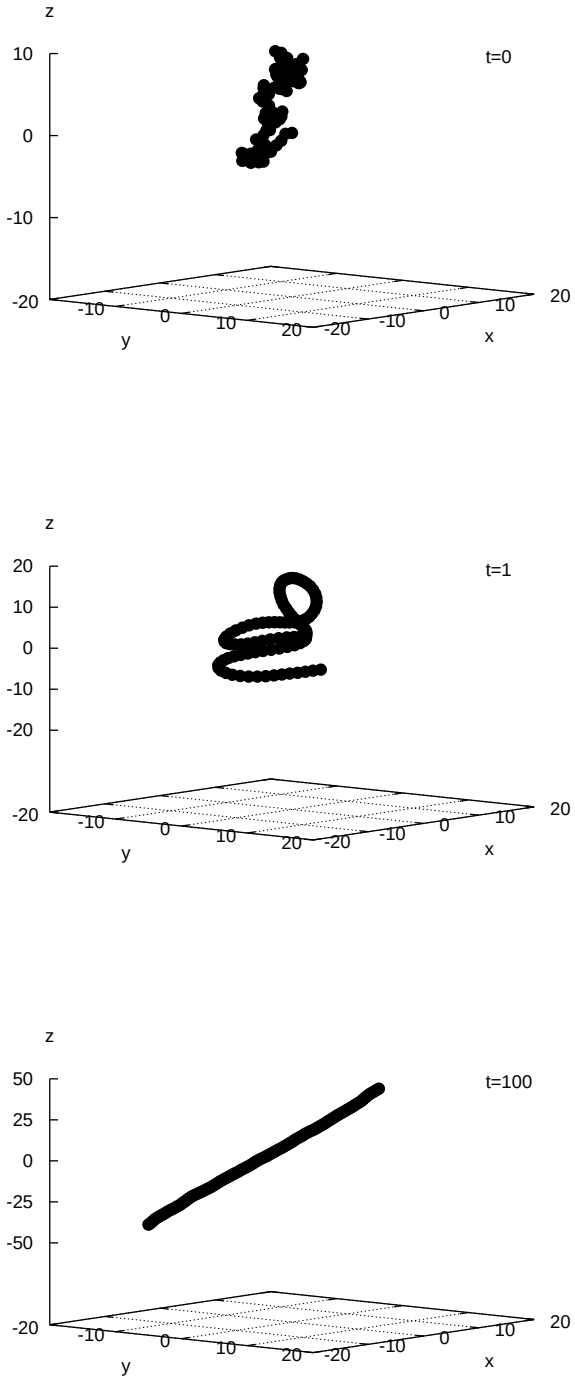

Figure 5.1: Stiffening of a N=100 polymer chain from an initial coiled state (t/τ_{rand} =0) to its intermediate helical shape (t/τ_{rand} =1) followed by the final stiff configuration with E=1000 (t/τ_{rand} =100).

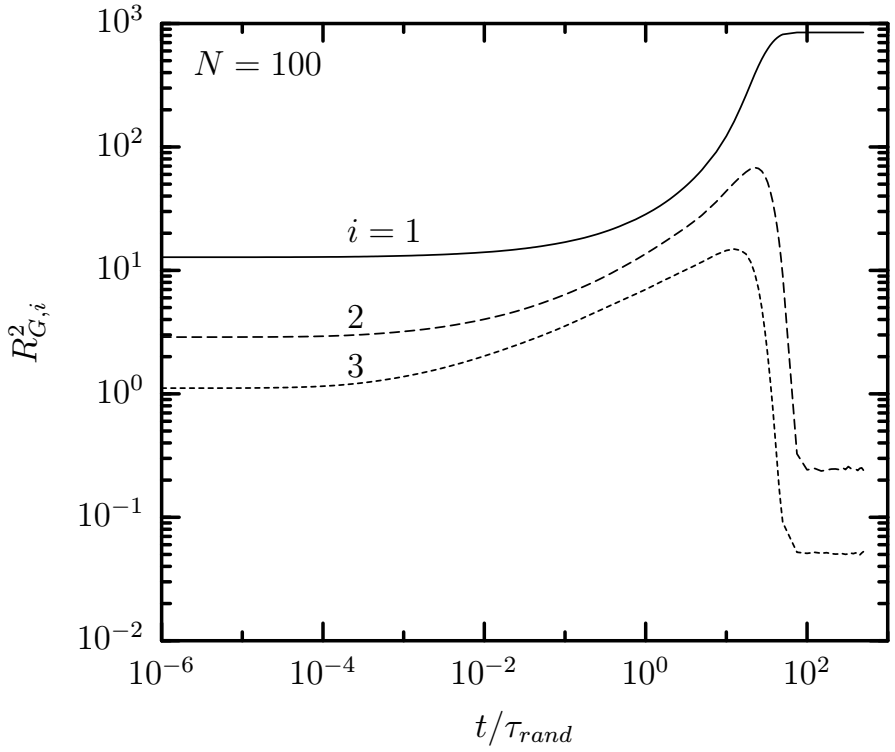

Figure 5.2: Eigenvalues from the gyration tensor, $E/N = 10$.

To understand the short-time and intermediate-time dynamics we determine scaling laws for the chain length, the chain width, and the first normal stress. Chains lengths up to $N = 100$ have been studied, covering stiffness ratios from $E/N = 0.1$ to $E/N = 100$. We have successfully determined the universal stiffening behavior of the three properties. Because the scaling laws account for the stiffness ratio, E/N, our results are universal for all stiffness ratios studied.

Figure 5.3 presents the short and intermediate-time scaling behavior of the first eigenvalue. As seen in figure 5.3(a), free diffusion of the chains is present. The short-time scale is seen to be linear with respect to the bending energy

$$\Delta R_{G,1}^2 \sim tE. \tag{1}$$

The intermediate scaling seen in figure 5.3(b), shows a 1/2 power law growth resulting in the following scaling law

$$\Delta R_{G,1}^2 \sim t^{1/2} E^{1/2}. \tag{2}$$

Upon examining the scaling behavior of the chain width, we see similar behavior; figures 5.4(a) and 5.4(b) respectively, show the short-time free diffusion and the intermediate power law growth of 1/2. The universal scaling laws for the chain width can be described by Eq (1) and Eq (2). Both the chain length and width have been reduced with respect to their zero-time value to arrive at the concluded

scalings. The matching behavior of the two eigenvalues describe the isotropic nature of the stiffening process.

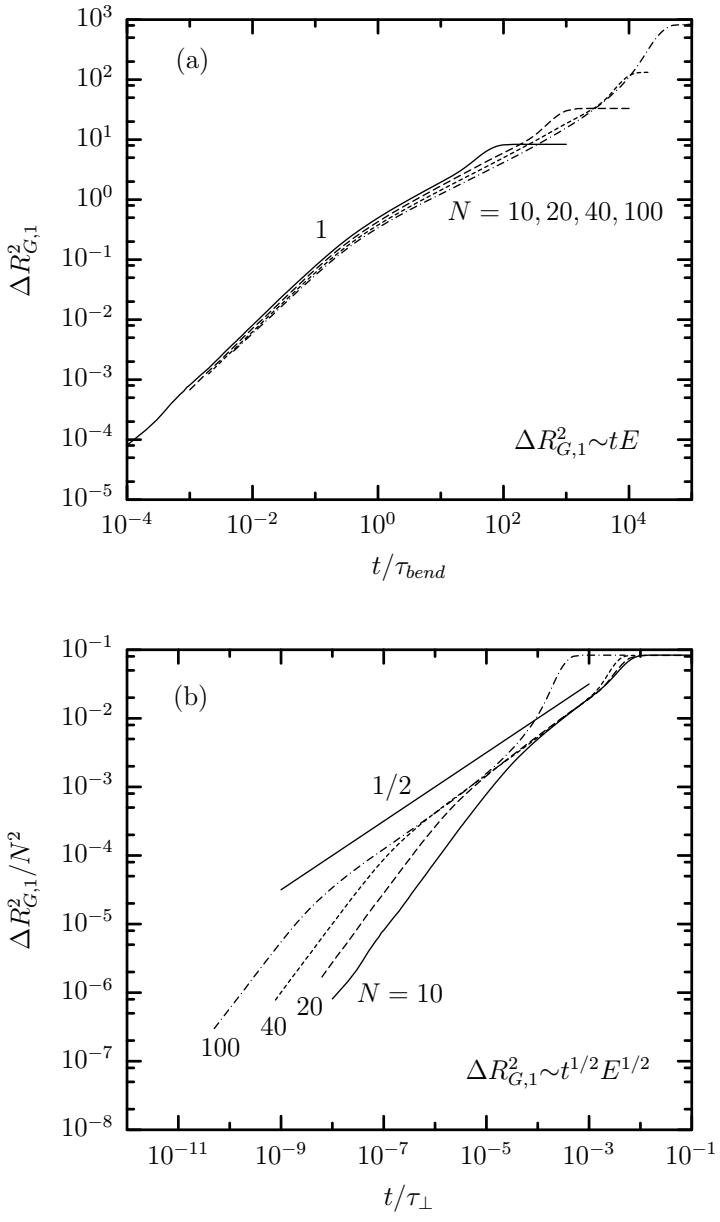

Figure 5.3: Universal scaling laws for the chain length at (a) short and (b) intermediate-times. The stiffening behavior for E/N=0.1,1,10,100 is shown. Note that $\Delta R^2_{G,i} = R^2_{G,i}(t) - R^2_{G,i}(0)$.

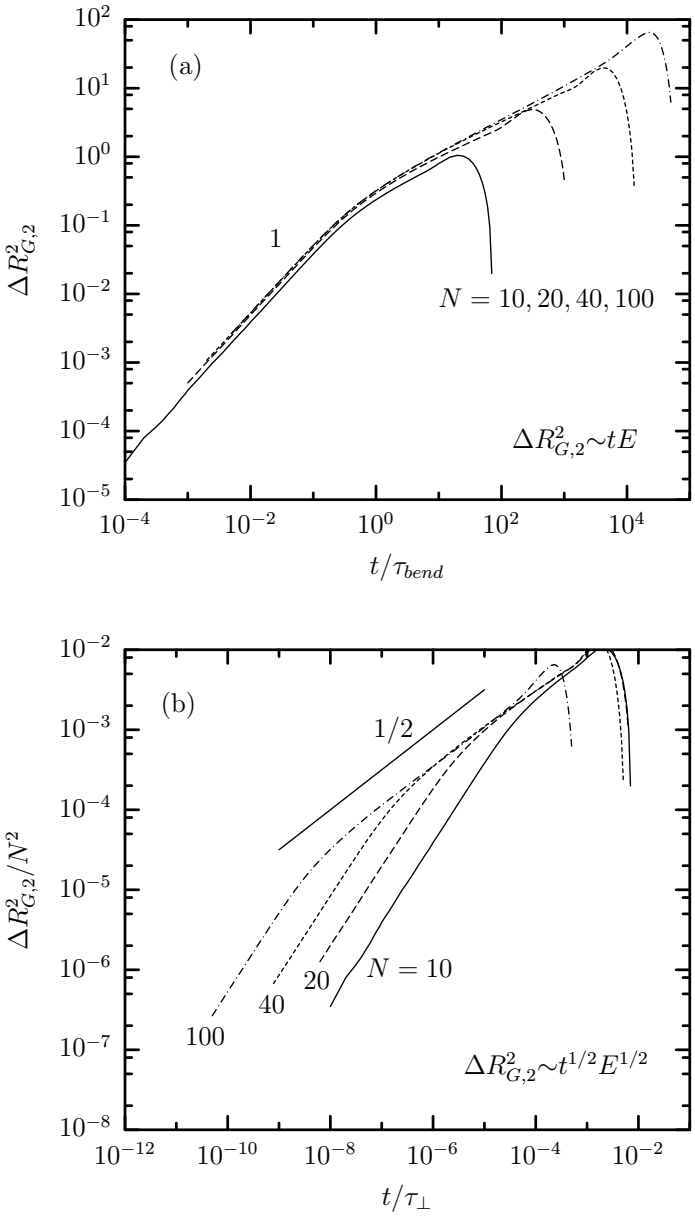

Figure 5.4: Universal scaling laws for the chain width at (a) short and (b) intermediate-times. The stiffening behavior for E/N=0.1,1,10,100 is shown. Note that $\Delta R^2_{G,i} = R^2_{G,i}(t) - R^2_{G,i}(0)$.

Finally, the dynamics of the first normal stress component can be seen in figure 5.5. We can notice the effect of both chain length and rigidity on the zero-time stress behavior. Figure 5.5(a) predicts a short-time stress scaling of

$$\sigma_n \sim (N\ link)\ X\ (E\ per\ link). \tag{3}$$

As seen in figure 5.5(b) at intermediate-times a power law decay of -0.5 is experienced by the chain resulting in an intermediate-time scaling such that

$$\sigma_n \sim N t^{-1/2} E^{1/2}. \tag{4}$$

We confirm the normal stress behavior by looking at the behavior of the chain length. The isotropic growth seen by the chain's length and width reveals the normal force acting on the macromolecule at short-time,

$$F_n \sim N \frac{d(\Delta R_{G,1})}{dt} \sim N\, t^{-1/2} E^{1/2} \tag{5}$$

knowing this we predict the corresponding short-time normal stress

$$\sigma_n \sim\ \Delta R_{G,1} F_n\ \sim NE. \tag{6}$$

A similar intermediate-time analysis yields,

$$F_n \sim N\frac{d(\Delta R_{G,1})}{dt} \sim N\,t^{-3/4}E^{1/4} \tag{7}$$

$$\sigma_n \sim \Delta R_{G,1}F_n \sim Nt^{-1/2}E^{1/2}. \tag{8}$$

As expected, both analytical results are in agreement with the numerical behavior predicted in Eq. (3) and Eq. (4) based on the data in figure 5.5.

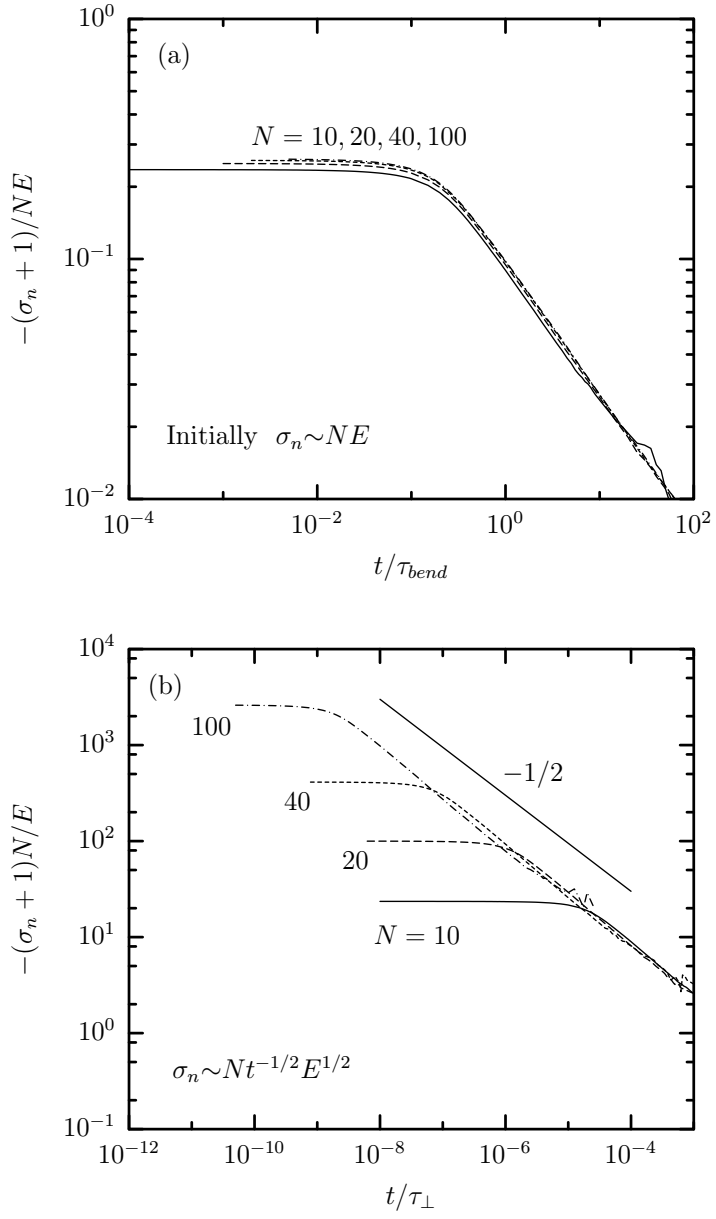

Figure 5.5: Universal scaling laws for the chain width at (a) short and (b) intermediate-times. The stiffening behavior for E/N=0.1,1,10,100 is shown.

Chapter 6

Conclusions

Semiflexible polymer molecules exhibit complex physical behaviors when subjected to different solution conditions. The effect of forces on dilute chain dynamics has been studied. The focus of this research was to understand the non-Newtonian properties of single semiflexible polymer molecules under transient relaxation and stiffening conditions. Through computational modeling we were able to predict the various dynamics covering most time scales experienced by the macromolecule. With a Brownian dynamics algorithm, we have conducted the nonequilibrium studies on chains of varying lengths and rigidity.

The dynamic behavior of a bead-rod chain was monitored as it relaxed from an initially extended state. In past works, Brownian dynamics nonequilibrium relaxation studies were limited to short chains and focused predominately on the stress and birefringence behavior of flexible chains at short times. Through scaling

law analysis universal relaxation laws were determined for semiflexible chains. A correlation was found such that the properties studied can be based on the single parameter of chain length. The transient properties and conformations adopted by long stiff chains in solution have also been examined. Studies of the relaxation behavior show the long chains exhibiting two intermediate-time behaviors due to the presence of bending energy. We conclude the eigenvalues of the gyration tensor are a valuable tool towards the understanding of polymer deformation in solution. Not only were we able to identify polymer shape changes, but we also were able to use the chain length to predict other chain properties, such as stress and birefringence, as well as to derive a nonlinear stress-optic law valid for stiff chains and all time scales.

The second project, similar to the first, describes the detailed simulation method and results for the relaxation of a nearly extended worm-like chain. The short and intermediate-time relaxation for bead-spring chains with $b_k = 0.005$ was observed. We find the worm-like chain model predicts the short-time free diffusion seen for bead-rod chains. A disadvantage of this model is the small time step required. The differences between the two chain models can be seen with the short-time stress scaling. The bead-rod stress is on the order of N^3 while the WLC model depends on the elasticity and scales as Nb_k^2. Another main difference can be noticed in the behavior of the chain width. Unlike the bead-rod model where the link lengths are fixed, there is no preservation of the spring lengths. This

is especially noticeable in the behavior of the chain width, where a continuous growth is seen even at intermediate times.

Finally, the coil-helix-rod stiffening behavior was successfully followed via Brownian dynamics simulations. In this study, we show that the chain evolves from a flexible coil to a rigid rod by first going through an intermediate helical shape change, especially noticeable in the longer chains. The influence of the bending energy on chain properties such as the chain length, width, and stress was also predicted for both short and intermediate-times.

Brownian dynamics of a series of different dilute solution conditions and polymer models has been presented. The simulation of polymers under various solution conditions has furthered our understanding of polymer structure to property relationships. An advantage of computer simulations is the ability to control the interactions of the system. An important conclusion that we draw from these studies is that the configuration behavior of the chain can be used to infer the scaling of other chain properties such as stress, birefringence, or tensions. Through parallel computation we were able to study chains much longer than previous studies and cover a wide range of stiffnesses.

Chapter 7

Future Work

There are several avenues that should be further explored; namely the extension behavior of bead-rod chains and the stiffening dynamics of WLC.

An understanding of the macromolecule's properties would not be complete without studying the chain behavior at extension. The goal of this study would be to explain the full transient behavior of chain deformation and orientation under extensional flow. Studying the physics of this problem can provide insight towards developing molecular models and relevant equations relating chain properties subjected to an external stretching force.

Following the behavior of the chain as it approaches equilibrium is just as important as following the behavior of the chain as it diverges from equilibrium. This study will help towards understanding chain deformation and its subsequent effect on chain properties. As the chain is being stretched by an extensional

flow, the chain properties and associated time scales can be monitored to further understand chain deformation and orientation under this linear flow. The influence of flow on polymer chains is of interest due to the solution's non-Newtonian nature. Understanding chain deformation and dynamics has been an ongoing study for many decades [11, 42] and there is still more to be understood, especially material behavior and manipulation in microfluidics and other nanotechnology systems.

The study of extensional flow is especially of interest because of its ability to deform the chain greatly away from equilibrium. Under the influence of extensional flow, when the drag force exceeds the Brownian forces, a coil-stretch transition is noticed. Chain properties such as the radius of gyration, viscosity and birefringence stay unaffected remaining close to their equilibrium (no-flow) value until a critical strain rate is passed, then a sharp growth in chain size, viscosity or birefringence is noticed [9, 19, 70]. This change is due to the polymer transitioning from that of a coiled chain to a stretched chain. The critical strain rate has been found to be dependent on the chain length and on hydrodynamic interactions (HI) [9, 46].

Starting with a random chain configuration, single chains can be fully extended through the presence of a strong extensional or shear flow. This can be compared to experimental studies involving attaching one end of the macromolecule to a bead and then exerting a flow field past the tethered end [56, 57, 64]. Previous results with flexible chains under extensional flow demonstrate that the chains

undergo many conformational stages ranging from folds, kinks, dumbbells, to a final extended state [19, 44, 57, 64]. Larson *et al.* [44] not only studied the unraveling dynamics of single flexible polymer chains but also compared results to the recent experimental findings of Perkins *et al.* and Smith *et al.* [57, 64]. Excellent agreement was noted. They were also able to confirm that the initial conformation of the chain does dominate the unraveling path it takes.

Even though the effects of extension on the dynamics of the polymer chain has been studied both experimentally and through simulations, the studies are limited to flexible chains. The effect of an extensional flow field on chains of varying length and rigidity can be studied over extended time periods through parallel computation. To see the influence on the physics and evolution of the chain's time scales, the flow strength can also be a variable of interest. Since, after a long enough time period the chain will be at an extended state, our experience on the relaxation of initially straight bead-rod chains will be useful to understanding the long-time semiflexible behavior of this problem. The reverse behavior from relaxation is not expected due to the different mechanics and the non-linear dynamics involved [9, 27].

Another possible study includes further investigating the WLC relaxation study; i.e., looking at chain properties such as birefringence to understand the optical behavior of the model compared to the bead-rod results, or understanding the effect of the Kuhn length on the chain dynamics and forces involved at near

extension. Studying the effect of flexibility on the chain properties for a constant chain length may also be explored. Because the chain length will be held constant we expect the zero time value, for both chain length and width to be independent of b_k. The intermediate-time relaxation of the eigenvalues will be dependent on the stiffness, such that the most elastic chain will come to equilibrium faster than the more rigid chain. However, unlike the behavior of the chain lengths, one would expect the initial stress to be dependent on the chain's Kuhn length. An inverse dependence is predicted because of the inverse relationship between the spring force and b_k. The polymer field of study is rich with interesting physics; many possibilities exist for future studies for this class of material.

Bibliography

[1] D.B. Adolf and M.D. Ediger. Brownian dynamics simulations of local motions in polyisoprene. *Macromolecules* **24**, 5834–5842, 1991.

[2] U.S. Agarwal, R. Bhargava, and R.A. Mashelkar. Brownian dynamics simulation of a polymer molecule in solution under elongational flow. *J. Chemical Physics* **108**, 1610–1617, 1998.

[3] U.S. Agarwal. Effect of initial conformation, flow strength, and hydrodynamic interaction on polymer molecules in extensional flows. *J. Chemical Physics* **113**, 3397–3403, 2000.

[4] N.C. Andrews, A.J. McHugh, and J.D. Schieber. Conformational and rheological dynamics of semiflexible macromolecules undergoing shear flow: a nonequilibrium brownian dynamics study. *J. Rheology* **42**, 281–305, 1998.

[5] C.G. Baumann, S.B. Smith, V.A. Bloomfield, and C. Bustamante. Ionic effects on the elasticity of single DNA molecules. *Proc. Natl. Acad. Sci.* **94**, 6185–6190, 1997.

[6] R.B. Bird, R.C. Armstrong, and O. Hassager. *Dynamics of polymeric liquids Vol. 1.* John Wiley & Sons, 1987.

[7] C. Bouchiat, M.D. Wang, J.F. Allemand, T. Strick, S.M. Block, and V. Croquette. Estimating the persistence length of a worm-like chain molecule from force-extension measurements. *Biophysical Journal* **76**, 409–413, 1999.

[8] C. Bustamante, J.F. Marko, E.D. Siggia, and S. Smith. Entropic elasticity of l-phage DNA. *Science* **265**, 1599–1600, 1994.

[9] J.G.H. Cifre and J.G. de la Torre. Simulation of polymers in dilute solution under elongational flow. *J. Non-Crystalline Solids* **235-237**, 717–722, 1998.

[10] J.G.H. Cifre and J.G. de la Torre. Steady-state behavior of dilute polymers in elongational flow. Dependence of the critical elongational rate on chain length, hydrodynamic interaction, and excluded volume. *J. Rheology* **43**, 339–358, 1999.

[11] P.G. De Gennes. Coil-stretch transition of dilute flexible polymers under ultrahigh velocity gradients. *J. Chemical Physics* **60**, 5030–5042, 1974.

[12] E.W. Dent and F.B. Gertler. Cytoskeletal dynamics and transport in growth cone motility and axon guidance. *Neuron* **40**, 209–227, 2003.

[13] P. Dimitrakopoulos, J.F. Brady, and Z.-G. Wang. Short- and intermediate-time behavior of the linear stress relaxation in semiflexible polymers. *Physical Rev. E* **64** (5), 050803, 2001.

[14] P. Dimitrakopoulos. Conformational evolution of initially straight flexible and stiff polymers over extended time periods via the scaling law methodology. *J. Chemical Physics* **119** (15), 8189–8196, 2003.

[15] P. Dimitrakopoulos. Stress and configuration relaxation of an initially straight flexible polymer. *J. Fluid Mechanics* **513**, 265–286, 2004.

[16] P. Dimitrakopoulos. Longitudinal relaxation of initially straight flexible and stiff polymers. *Physical Rev. Letters* **93**, 217801, 2004.

[17] I.D. Dissanayake and P. Dimitrakopoulos. Stress, birefringence and conformational relaxation of initially straight stiff bead-rod polymer. *Physical Rev. E*, **under-review**.

[18] I.D. Dissanayake and P. Dimitrakopoulos. Dynamics of biological and synthetic polymers through large-scale parallel computations. *Parallel Computational Fluid Dynamics: Theory and Practice*

[19] P.S. Doyle, E.S.G. Shaqfeh, and A.P. Gast. Dynamic simulation of freely draining flexible polymers in steady linear flows. *J. Fluid Mechanics* **334**, 251–291, 1997.

[20] P.S. Doyle and E.S.G. Shaqfeh. Dynamic simulation of freely-draining, flexible bead-rod chains; start-up of extensional and shear flow. *J. Non-Newton Fluid Mechanics* **76**, 43–78, 1998.

[21] P.S. Doyle, E.S.G. Shaqfeh, G.H. McKinley, and S.H. Spiegelberg. Relaxation of dilute polymer solutions following extensional flow. *J. Non-Newton Fluid Mechanics* **76**, 79–110, 1998.

[22] M. Doi and S.F. Edwards. *The theory of polymer dynamics*. Clarendon, Oxford, 1986.

[23] T.H. Duong and K. Zakrzewska. Influence of drug binding on DNA flexibility: A normal mode analysis. *J. of Biomolecular Structure and Dynamics* **14**, 691–701, 1997.

[24] G.G. Fuller. Optical rheometry. *Annu. Rev. Fluid Mechanics* **22**, 387–417, 1990.

[25] G.G. Fuller. *Optical Rheometry of Complex Fluids*. Oxford University Press, 1995.

[26] J. Gao and J.H. Weiner. Computer simulations of viscoelasticity in polymer melts. *Macromolecules* **25**, 1348–1356, 1992.

[27] I. Ghosh, G.H. McKinley, R.A. Brown, and R.C. Armstrong. Deficiencies of FENE dumbbell models in describing the rapid stretching of dilute polymer solutions. *J. Rheology* **45**, 721-758, 2001.

[28] I. Ghosh, Y.L. Joo, G.H. McKinley, R.A. Brown, and R.C. Armstrong. A new model for dilute polymer solutions in flows with strong extensional components. *J. Rheology* **46**, 1057-1089, 2002.

[29] R.E. Goldstein and S.A. Langer. Nonlinear dynamics of stiff polymers. *Physical Rev. Letters* **75**, 1094–1097, 1995.

[30] Y.Y. Gotlib and L.I. Klushin. Dynamics of irreversible uncoiling of a polymer chain. *Polymer* **32**, 3408–3414, 1991.

[31] J.W. Hatfield and S.R. Quake. Dynamic properties of an extended polymer in solution. *Physical Rev. Letters* **82** (17), 3548–3551, 1999.

[32] E.J. Hinch. Uncoiling a polymer molecule in a strong extensional flow. *J. Non-Newton Fluid Mechanics* **54**, 209–230, 1994.

[33] P.S. Grassia and E.J. Hinch. Computer simulation of polymer chain relaxation via brownian motion. *J. Fluid Mechanics* **308**, 255–288, 1996.

[34] R.M. Jendrejack, J.J. de Pablo, and M.D. Graham. Stochastic simulations of DNA in flow: Dynamics and the effects of hydrodynamic interactions. *J. Chemical Physics* **116**, 7752–7759, 200.

[35] J.P. Kemp and Z.Y. Chen. Formation of helical states in wormlike polymer chains. *Physical Rev. Letters* **81**, 3880–3883, 1998.

[36] J.P. Kemp and J.Z.Y. Chen. Helical structures in proteins. *Biomacromolecules* **2**, 389–401, 2001.

[37] J. Kierfeld and R. Lipowsky. Unbundling and desorption of semiflexible polymers. *Europhys. Letters* **62**, 285–291, 2003.

[38] K. Kremer and G.S. Grest. Dynamics of entangled linear polymer melts: A molecular-dynamics simulation. *J. Chemical Physics* **92**, 5057–5086, 1990.

[39] S.J. Kron and J.A. Spudich. Fluorescent actin filaments move on myosin fixed to a glass surface. *Proc. Natl. Acad. Sci. USA* **83**, 6272–6276, 1986.

[40] T.C.B. Kwan, N.J. Woo, and E.S.G. Shaqfeh. An experimental and simulation study of dilute polymer solutions in exponential shear flow: Comparison to uniaxial and planar extensional flows. *J. Rheology* **45**, 321–349, 2001.

[41] B. Ladoux and P.S. Doyle. Stretching tethered DNA chains in shear flow. *Europhys. Letters* **52**, 511–517, 2000.

[42] R.G. Larson and J.J. Magda. Coil-stretch transition in mixed shear and extensional flows of dilute polymer solutions. *Macromolecules* **22**, 3004–3010, 1989.

[43] R.G. Larson, T.T. Perkins, D.E. Smith, and S. Chu. Hydrodynamics of a DNA molecule in a flow field. *Physical Rev. E* **55**, 1794–1797, 1997.

[44] R.G. Larson, H. Hu, D.E. Smith, and S. Chu. Brownian dynamics simulations of a DNA molecule in an extensional flow field. *J. Rheology* **43**, 267–304, 1999.

[45] L. Li and R.G. Larson. Comparison of brownian dynamics simulations with microscopic and light-scattering measurements of polymer deformation under flow. *Macromolecules* **33**, 1411–1415, 2000.

[46] S. Liu, B. Ashok, and M. Muthukumar. Brownian dynamics simulations of bead-rod chain in simple shear flow and elongational flow. *Polymer* **45**, 1383–1389, 2004.

[47] J.F. Marko and E.D. Siggia. Stretching DNA. *Macromolecules* **28**, 8759–8770, 1995.

[48] P.Y. Meadows, J.E. Bemis, and G.C. Walker. Single-molecule force spectroscopy of isolated and aggregated fibronectin proteins on negatively charged surfaces in aqueous liquids. *Langmuir* **19**, 9566–9572, 2003.

[49] J. Meiners and S.R. Quake. Femtonewton force spectroscopy of single extended DNA molecules. *Physical Rev. Letters* **84**, 5014–5017, 2000.

[50] T.Q. Nguyen and H-H Kausch. *Flexible polymer chains in elongational flow.* Springer, 1999.

[51] M. Nisoli, A. Cybo-Ottone, S. De Silvestri, and V. Magni. Femtosecond transient absorption saturation in poly (alkyl-thiophene-vinylene)s. *Physical Rev. B* **47**, 10881–10884, 1993.

[52] C.K. Ober. Shape persistence of synthetic polymers. *Science* **288**, 448–449, 2000.

[53] Q. Peng, M.Q. Xie, Y. Huang, Z.Y. Lu, and Y. Cao. Novel supramolecular polymers based on zinc-salen chromophores for efficient light-emitting diodes. *Macromolecular Chemistry and Physics* **206**, 2373–2380, 2005.

[54] T.T. Perkins, D.E. Smith, and S. Chu. Direct observation of tube-like motion of a single polymer chain. *Science* **264**, 819–822, 1994.

[55] T.T. Perkins, S.R. Quake, D.E. Smith, and S. Chu. Relaxation of a single DNA molecule observed by optical microscopy. *Science* **264**, 822–826, 1994.

[56] T.T. Perkins, D.E. Smith, R.G. Larson, and S. Chu. Stretching of a single tethered polymer in a uniform flow. *Science* **268**, 83–87, 1995.

[57] T.T. Perkins, D.E. Smith, and S. Chu. Single polymer dynamics in an elongational flow. *Science* **276**, 2016–2021, 1997.

[58] S.S. Ray and M. Bousmina. Biodegradable polymers and their layered silicate nano composites: In greening the 21st century materials world. *Progress in Materials Science* **50**, 962–1079, 2005.

[59] Y. Rouault. The effect of stiffness in wormlike micelles. *European Physical Journal B* **6**, 75–81, 1998.

[60] T. Sakaue and K. Yoshikawa. Folding/unfolding kinetics on a semiflexible polymer chain. *J. Chemical Physics* **117**, 6323–6330, 2002.

[61] V. Schmitt, F. Lequeux, and C.M. Marques. Confinement of dilute solutions of living polymers. *J. Phys. II France* **3**, 891–902, 1993.

[62] V. Shankar, M. Pasquali, and D.C. Morse. Theory of linear viscoelasticity of semiflexible rods in dilute solution. *J. Rheology* **46**, 1111–1154, 2002.

[63] E.S.G. Shaqfeh, G.H. McKinley, N. Woo, D.A. Nguyen, and T. Sridhar. On the polymer entropic force singularity and its relation to extensional stress relaxation and filament recoil. *J. Rheology* **48**, 209–221, 2004.

[64] D.E. Smith and S. Chu. Response of flexible polymers to a sudden elongational flow. *Science* **281**, 1335–1340, 1998.

[65] D.E. Smith, H.P. Babcock, and S. Chu. Single-polymer dynamics in steady shear flow. *Science* **283**, 1724–1727, 1999.

[66] M. Somasi, B. Khomami, N.J. Woo, J.S. Hur, and E.S.G. Shaqfeh. Brownian dynamics simulations of bead-rod and bead-spring chains: Numerical algorithms and coarse-graining issues. *J. Non-Newton Fluid Mechanics* **108**, 227–255, 2002.

[67] A.J. Spakowitz and Z.-G. Wang. Free expansion of elastic filaments. *Physical Rev. E* **64**, 061802, 2001.

[68] K. Terao, Y. Terao, A. Teramoto, N. Nakamura, M. Fujiki, and T. Sato. Temperature and solvent dependence of stiffness of polyn-hexyl-[(S)-3-methylpentyl]silylene in dilute solutions. *Macromolecules* **34**, 4519–4525, 2001.

[69] J.R. Wenner, M.C. Williams, I. Rouzina, and V.A. Bloomfield. Salt dependence of the elasticity and overstretching transition of single DNA molecules. *Biophysical Journal* **82**, 3160–3169, 2002.

[70] J.M. Wiest. Birefringence in strong flows of polymer solutions. *Polymer* **40**, 1917–1922, 1999.

[71] H.R. Warner. Kinetic theory and rheology of dilute suspensions of finitely extensible dumbbells. *Ind. Eng. Chem. Fundam.* **11**, 379-387, 1972.